PHYSICAL REVIEW D **94,** 055022 (2016)

Dimension-seven operators in the standard model with right handed neutrinos

Subhaditya Bhattacharya[1,*] and José Wudka[2,†]

[1]*Department of Physics, Indian Institute of Technology Guwahati, Guwahati, Assam 781039, India*
[2]*Department of Physics and Astronomy, University of California Riverside, Riverside, California 92521-0413, USA*

(Received 9 February 2016; published 19 September 2016)

In this article, we consider the standard model extended by a number of (light) right-handed neutrinos, and assume the presence of some heavy physics that cannot be directly produced, but can be probed by its low-energy effective interactions. Within this scenario, we obtain all the gauge-invariant dimension-7 effective operators, and determine whether each of the operators can be generated at tree level by the heavy physics, or whether it is necessarily loop generated. We then use the tree-generated operators, including those containing right-handed neutrinos, to put limits on the scale of new physics Λ using low-energy measurements. We also study the production of same-sign dileptons at the Large Hadron Collider and determine the constraints on the heavy physics that can be derived from existing data, as well as the reach in probing Λ expected from future runs of this collider.

DOI: 10.1103/PhysRevD.94.055022

I. INTRODUCTION

The standard model (SM) is generally believed to be the low-energy limit of a more fundamental theory; however, the presence of new physics (NP) has eluded almost all experiments to date, the notable exceptions being the observation of neutrino masses [1] and the very strong evidence that dark matter [2] is composed of particle(s) not present in the SM. Because of this paucity of experimental guidance on even the most basic properties of NP, it is reasonable to study the effects of hypothesized heavy particles using a model-independent approach based on an effective theory. Using this approach, one can derive reliable bounds (or estimates) of some of the most important parameters of physics beyond the SM (such as its scale) and map such constraints onto specific models of NP. The procedure for constructing an effective Lagrangian is well known [3–5], and though some important details depend on whether the NP is assumed to be strongly [5] or weakly [6] coupled, in either case the formalism provides an efficient and consistent parametrization of all heavy-physics effects at scales below that of the NP.

The recent observation of the Higgs boson with a mass below the electroweak scale strongly suggests that the electroweak sector of the SM is weakly coupled. This also supports the assumption that any NP underlying the SM is also weakly coupled and, since the SM Lagrangian is renormalizable [7], decoupling [8]. We will adopt these assumptions in this paper, but they are certainly not inescapable: the observed Higgs particle may not be exactly the particle predicted by the SM (e.g. the scalar sector might contain other fields) [9], and it is possible to construct models of strongly coupled new physics that are consistent with a weakly coupled SM [10].

The action for the effective theory, $S_{\rm eff}$, results from integrating out all heavy modes in the full theory. By construction, $S_{\rm eff}$ will contain only SM fields, and by consistency will respect all the SM local symmetries [11]; it will also depend on the parameters of the NP and, in particular, on the typical heavy-physics scale Λ. Expanding in powers of Λ, we can write $S_{\rm eff}$ as the integral of a local effective Lagrangian; the decoupling assumption guarantees that terms with positive powers of Λ are absorbed in renormalization of the low-energy theory (in this case, the SM), so that all observable NP effects are suppressed by inverse powers of Λ. Thus, we can write

$$\mathcal{L}_{\rm eff} = \mathcal{L}_{\rm SM} + \sum_{i,n\geq 5} \frac{c_i^{(n)}}{\Lambda^{n-4}} \mathcal{O}_i^{(n)}, \tag{1}$$

where the $\mathcal{O}_i^{(n)}$ are gauge-invariant local operators with mass dimension n constructed using SM fields and their derivatives, and the $c_i^{(n)}$ are unknown coefficients.[1] It is important to note that, though it is not indicated in the above expressions, different operators may be generated by NP of different scales (in the above notation, Λ can depend on the index i), but we will not indicate this explicitly so as not to clutter the expressions. Although the effective Lagrangian in Eq. (1) formally contains an infinite number

*subhab@iitg.ernet.in
†jose.wudka@ucr.edu

[1]If the NP Lagrangian were known, these coefficients could be calculated; absent this, we take them as unknown quantities parametrizing the physics beyond the SM, and which can be experimentally measured or constrained.

of coefficients, only operators of sufficiently small dimension, corresponding to a finite number of terms, can generate effects large enough to be measured within experimental accuracy. Hence, the effective Lagrangian approach does not suffer from lack of predictability, and is useful when the nature of the NP is not known very well, as in the present situation in particle physics.

There are publications providing complete lists of operators of dimensions $n = 5, 6, 7$ [12–15] and partial lists of operators with $8 \leq n \leq 11$ [16]; using these results, very many studies have been published (see, e.g. Refs. [17,18]) that obtain limits on Λ using a variety of processes.

As mentioned above, one type of new physics that has been confirmed is the existence of neutrino masses, yet the mechanism responsible for them is not determined. One popular possibility is that these masses are of the Majorana type [19], assumed to be generated by lepton-number-violating NP[2] without requiring additional light degrees of freedom. An alternative possibility is for the lepton sector to mimic the quark sector as far as mass generation is concerned; in this case, it is assumed that there are three right-handed light neutrinos ν_R that pair up with their left-handed counterparts and generate Dirac masses in the usual manner.

Both cases can be studied simultaneously by including the ν_R in the set of SM fields that are used to construct the effective Lagrangian; we will denote this model by νSM. We emphasize that these right-handed neutrinos are assumed to be light—the effects of heavy right-handed neutrinos are included through the appropriate effective operators.

The list of effective operators for the νSM extension of the SM are available for dimensions 5 and 6 [20,21]. Despite the increased suppression by powers of Λ, dimension-7 operators remain relevant because of their contributions to interesting processes, such as neutrinoless double-beta decay [22], so that a complete list of dimension-7 operators for the νSM will be useful in this context. The goal of this publication is to provide such a list and to analyze some of the observables sensitive to the corresponding types of NP.

When the physics underlying the SM is weakly coupled, it is useful to note that, in addition to the suppression in powers of Λ, the effective operator coefficients will be further reduced when the corresponding operator is not generated at tree level. It is an interesting property of renormalizable NP models that there are effective operators that are never generated at tree level [23]; we will call these *loop-generated* (LG) operators. The remaining operators may or may not be generated at tree level, depending on the details of the NP; we refer to these as *potentially tree-generated* (PTG) operators. This separation is of interest because the effects of LG operators are almost always too small to be of interest, being smaller than the one-loop SM corrections; exceptions do occur in cases where there is no SM contribution at tree level (e.g. in Higgs production via gluon fusion or the two-photon and Z-photon decay modes [24]). Because of this, processes to which PTG operators contribute are generally the ones most sensitive to the effects of heavy physics [23].

In practical applications of the effective theory approach, it is useful to note that the effects of some operators cannot be distinguished using only low-energy observables [6], and that this allows dropping some of the terms in Eq. (1). Specifically, if two operators $\mathcal{O}, \mathcal{O}'$ are such that the linear combination $\mathcal{O} + r\mathcal{O}'$ is zero on shell, and they appear in the effective Lagrangian in the combination $c\mathcal{O} + c'\mathcal{O}'$, then all observables will depend on c and c' only through the combination $c' - rc$. In this sense, the effects of $\mathcal{O}$ and $\mathcal{O}'$ cannot be distinguished, and either of them can be eliminated from $\mathcal{L}_{\text{eff}}$. (For details, see Refs. [6,14]; this result is often referred to as the "equivalence theorem" [6].) Once redundant operators are eliminated through this procedure, the remaining ones constitute an irreducible basis. In choosing a basis, it is usually more useful to select the ones with the largest number of PTG operators (for a full discussion, see Ref. [25]).

II. νSM DIMENSION-SEVEN OPERATORS

In this section, we provide a complete list of dimension-7 effective operators within the νSM. This list was obtained in a straightforward though tedious way, beginning from a general combination of fields and ensuring Lorentz and gauge invariance; the equations of motion were then used to eliminate redundant operators by applying the equivalence theorem [6,25]. For each of the operators listed, we will also indicate whether they are LG or PTG (as noted above, this is a relevant classification for the case where the underlying physics is weakly coupled, decoupling and renormalizable); in Appendix A, we present the arguments we used to obtain this classification.

In the expressions below, ϕ denotes the SM scalar isodoublet; ℓ a left-handed lepton isodoublet; q a left-handed quark doublet; e and ν right-handed charged and neutral leptons, respectively (we drop the subindex R to simplify the notation); and u and d right-handed up- and down-type quarks, respectively; we will for the most part suppress generation indices. We use D for the covariant derivatives and denote the $SU(3)_c, SU(2)_L$ and $U(1)_Y$ gauge fields by G, W and B, respectively. We will also use the shorthand

$$N = \phi^\dagger \epsilon \ell, \qquad E = \phi^\dagger \ell, \tag{2}$$

motivated by the fact that in the unitary gauge $N = (v/\sqrt{2})\nu_L + \cdots$, and $E = (v/\sqrt{2})e_L + \cdots$; we also use

[2]Specifically, at low energies, the heavy physics is assumed to generate the dimension-5 Weinberg operator $(\phi^\dagger \ell)^2$ [12] that produces the desired mass matrix upon spontaneous symmetry breaking.

$$\epsilon = -i\tau_2 = \begin{pmatrix} 0 & 1 \\ -1 & 0 \end{pmatrix}, \tag{3}$$

where τ_2 is the usual Pauli matrix and $v \sim 246$ GeV, the vacuum expectation value of the SM scalar doublet.

It is straightforward to show that in the νSM there are no dimension-7 operators without fermions; the operators containing two and four fermions are listed below.

A. Operators with two fermions

These operators are of the form[3]

$$\psi^T C\Gamma\psi'\varphi^r D^s, \qquad r+s=4, r, s \geq 0, \tag{4}$$

where φ denotes ϕ or $\tilde{\phi} = \epsilon\phi^*$; ψ a is fermion in the νSM,

$$\psi \in \{q, u, d, \ell, e, \nu, q^c, u^c, d^c, \ell^c, e^c, \nu^c\}; \tag{5}$$

C is the Dirac charge conjugation matrix; the charge conjugate fields are defined as $\psi^c = C\bar{\psi}^T$; and $\Gamma = \{1, \gamma^\mu, \sigma^{\mu\nu}\}$, where $\sigma^{\mu\nu} = \frac{i}{2}[\gamma^\mu, \gamma^\nu]$. All these operators conserve baryon number but violate lepton number by two units: $|\Delta L| = 2$, $\Delta B = 0$. (For an interesting discussion on operators with $|\Delta(B-L)| = 2$, neutrino masses and grand unification, see Ref. [26].)

(1) $r = 4$, $s = 0$. Two PTG operators:

$$(\overline{N^c}N)|\phi|^2, \qquad \overline{\nu^c}\nu|\phi|^4. \tag{6}$$

(2) $r = 3$, $s = 1$. Four PTG operators:

$$\begin{aligned} &(\overline{e^c}\gamma^\mu N)(\tilde{\phi}^\dagger \overleftrightarrow{D}_\mu \phi), \qquad (\overline{\nu^c}\gamma^\mu N)(i\phi^\dagger \overleftrightarrow{D}_\mu \phi), \\ &(\overline{\nu^c}\gamma^\mu E)(\tilde{\phi}^\dagger \overleftrightarrow{D}_\mu \phi), \qquad (\overline{\nu^c}\gamma^\mu N)(\partial_\mu|\phi|^2), \end{aligned} \tag{7}$$

where $\phi^\dagger \overleftrightarrow{D}_\mu \phi = \phi^\dagger D_\mu \phi - (D_\mu\phi)^\dagger\phi$.

(3) $r = s = 2$. Nine PTG operators:

$$\begin{aligned} &(\overline{\ell^c}D_\mu \ell)(\tilde{\phi}^\dagger D^\mu \phi), \qquad \overline{N^c}(D_\mu \tilde{\phi}^\dagger D^\mu \ell), \\ &(\overline{\ell^c}D\phi)(\ell\epsilon D\phi), \qquad [\overline{N^c}\sigma^{\mu\nu}(\tilde{\phi}^\dagger \mathbf{W}_{\mu\nu}\ell)], \\ &(\overline{\nu^c}D_\mu e)(\tilde{\phi}^\dagger D^\mu \phi), \qquad (\overline{\nu^c}\nu)|D\phi|^2, \\ &(\overline{\nu^c}\sigma^{\mu\nu}e)(\tilde{\phi}^\dagger \mathbf{W}_{\mu\nu}\phi), \qquad (\bar{N}^c\sigma^{\mu\nu}N)B_{\mu\nu}, \\ &|\phi|^2(\overline{\nu^c}\sigma^{\mu\nu}\nu)B_{\mu\nu}, \end{aligned} \tag{8}$$

where $\mathbf{W}_{\mu\nu} = \tau^I W^I_{\mu\nu}$.

[3]Field-strength tensors correspond to $[D, D]$ commutators contained in terms with $s = 2$ in Eq. (4).

TABLE I. Field combinations that can contribute to the operators [Eq. (11)] containing four fermions, one derivative and no scalar fields.

	L_1	L_2	L_3	R	ΔL	ΔB
1	d^c	d^c	d^c	e	1	−1
2	d^c	ℓ	ℓ	u	2	0
3	d^c	ℓ	d^c	q^c	1	−1
4	q	d^c	ℓ	ν	2	0
5	q	ℓ	d^c	ν	2	0
6	d^c	ℓ	q	ν	2	0
7	ℓ	e^c	ℓ	ν	2	0
8	q	u^c	ν^c	ℓ^c	−2	0
9	q	ν^c	u^c	ℓ^c	−2	0
10	u^c	ν^c	q	ℓ^c	−2	0
11	u^c	ν^c	e^c	d	−2	0
12	u^c	e^c	ν^c	d	−2	0
13	ν^c	e^c	u^c	d	−2	0
14	u^c	d^c	d^c	ν	1	−1
15	q	ν^c	q	d	−1	1
16	q	ν^c	ν^c	q^c	−2	0
17	u^c	ν^c	ν^c	u	−2	0
18	d^c	ν^c	ν^c	d	−2	0
19	ℓ	ν^c	ν^c	ℓ^c	−2	0
20	ν^c	e^c	ν^c	e	−2	0
21	ν^c	ν^c	ν^c	ν	−2	0

(4) $r = 1$, $s = 3$. Eight LG operators:

$$\begin{aligned} &(\partial^\mu\overline{\nu^c})\gamma^\nu N B_{\mu\nu}, \qquad \overline{\nu^c}\gamma^\mu(\tilde{\phi}^\dagger D^\nu \ell)B_{\mu\nu}, \\ &(\partial^\mu\overline{\nu^c})\gamma^\nu(\tilde{\phi}^\dagger \mathbf{W}_{\mu\nu}\ell), \qquad \overline{\nu^c}\gamma^\mu(\tilde{\phi}^\dagger \mathbf{W}_{\mu\nu}D^\nu \ell), \\ &(\partial^\mu\overline{\nu^c})\gamma^\mu N\tilde{B}_{\mu\nu}, \qquad \overline{\nu^c}\gamma^\mu(\tilde{\phi}^\dagger D^\nu \ell)\tilde{B}_{\mu\nu}, \\ &(\partial^\mu\overline{\nu^c})\gamma^\mu(\tilde{\phi}^\dagger \mathbf{W}_{\mu\nu}\ell), \qquad \overline{\nu^c}\gamma^\mu(\tilde{\phi}^\dagger \tilde{\mathbf{W}}_{\mu\nu}D^\nu \ell), \end{aligned} \tag{9}$$

where $\tilde{X}_{\mu\nu} = \frac{1}{2}\epsilon_{\mu\nu\rho\sigma}X^{\rho\sigma}$ denote the dual tensors.

(5) $r = 0$, $s = 4$. Six LG operators:

$$\begin{aligned} &\overline{\nu^c}\nu \times \{(G^A_{\mu\nu})^2, (W^I_{\mu\nu})^2, (B_{\mu\nu})^2, (\tilde{G}^A_{\mu\nu}G^A_{\mu\nu}), \\ &(\tilde{W}^I_{\mu\nu}W^I_{\mu\nu}), (\tilde{B}_{\mu\nu}B_{\mu\nu})\}. \end{aligned} \tag{10}$$

B. Operators with four fermions

These operators are of the form $\psi^4 D$ (operators with four fermions and one covariant derivative) or $\psi^4\varphi$ (operators with four fermions and one scalar); they all violate $|B-L|$ by two units with $|\Delta B| = 0, 1$.

(1) $\psi^4 D$: 21 LG operators. Using Fierz rearrangements, these can be cast in either of two forms:

$$(L_1\sigma^{\mu\nu}L_2)(L_3\gamma_\nu \overleftrightarrow{D}_\mu R), \qquad (L_1\sigma^{\mu\nu}L_2)D_\mu(L_3\gamma_\nu R), \tag{11}$$

where L and R denote left- and right-handed fermion fields, respectively. The allowed field combinations are listed in Table I.

TABLE II. Possible field combinations appearing in the four fermion operators containing one scalar and no derivatives [Eq. (12)]. The entries with one (two) asterisks have two (three) possible $SU(2)$ contractions (assuming only family-diagonal couplings; see text).

$\mathcal{O} = (L_1^T C L_2)(L_3^T C L_4)\varphi$							
	L_1	L_2	L_3	L_4	ΔL	ΔB	φ
1	ℓ	ℓ	ℓ	e^c	2	0	ϕ
2	q	d^c	ℓ	ℓ	2	0	ϕ
3**	q	ℓ	ℓ	d^c	2	0	ϕ
4	u^c	d^c	d^c	ℓ	1	−1	ϕ
5	d^c	d^c	d^c	ℓ	1	−1	$\tilde{\phi}$
6	u^c	ℓ	d^c	d^c	1	−1	ϕ
7	q	u^c	ν^c	e^c	−2	0	$\tilde{\phi}$
8	q	e^c	ν^c	u^c	−2	0	$\tilde{\phi}$
9*	q	q	q	ν^c	−1	1	$\tilde{\phi}$
10	q	u^c	ν^c	ν^c	−2	0	ϕ
11	q	d^c	ν^c	ν^c	−2	0	$\tilde{\phi}$
12	q	ν^c	ν^c	u^c	−2	0	ϕ
13	q	ν^c	ν^c	d^c	−2	0	$\tilde{\phi}$
14	ℓ	e^c	ν^c	ν^c	−2	0	$\tilde{\phi}$
15	ℓ	ν^c	ν^c	e^c	−2	0	$\tilde{\phi}$
16	ℓ	ν^c	ν^c	ν^c	−2	0	ϕ

$\mathcal{O} = (L_1^T C L_2)(R_1^T C R_2)\varphi$							
	L_1	L_2	R_1	R_2	ΔL	ΔB	φ
1	d^c	ℓ	u	e	2	0	ϕ
2	ℓ	ℓ	q^c	u	2	0	ϕ
3*	q	q	d	ℓ^c	−1	1	$\tilde{\phi}$
4	q	e^c	d	d	−1	1	$\tilde{\phi}$
5	q	d^c	ν	e	2	0	ϕ
6	u^c	ℓ	u	ν	2	0	ϕ
7	d^c	ℓ	u	ν	2	0	$\tilde{\phi}$
8	d^c	ℓ	d	ν	2	0	ϕ
9	ℓ	e^c	ν	e	2	0	ϕ
10**	q	ℓ	q^c	ν	2	0	ϕ
11	ℓ	ℓ	ℓ^c	ν	2	0	ϕ
12	q	ν^c	u	d	−1	1	$\tilde{\phi}$
13	q	ν^c	d	d	−1	1	ϕ
14	q	u^c	ν	ν	2	0	ϕ
15	q	d^c	ν	ν	2	0	$\tilde{\phi}$
16	ℓ	e^c	ν	ν	2	0	$\tilde{\phi}$
17	ℓ	ν^c	ν	ν	2	0	ϕ

(2) $\psi^4\phi$: 33 PTG operators. Using Fierz transformations, one can readily see that these take one of the following two forms:

$$(L_1^T C L_2)(L_3^T C L_4)\varphi, \quad (L_1^T C L_2)(R_1^T C R_2)\varphi, \qquad (12)$$

where $\varphi = \phi, \phi^c$. The allowed field combinations are listed in Table II.

The list of operators provided here does not include family labels to avoid notational clutter. In certain cases, however, the operators vanish when some of the fields are in the same family. For example, it is easy to see that $\ell^c C \ell = 0$ when both lepton isodoublets are in the same family, so any operators with this factor will not have family-diagonal contributions and should in principle be written as $\ell_i^c C \ell_j$, where $i, j = 1, 2, 3 (i \neq j)$ denote family indices. The contraction of the $SU(3)$ color indices is unambiguous in the above operators, since it can take only two forms: either $\{Q_r^c Q_s'\}\delta_{rs}$ or $\{Q_r^c Q_s'^c Q_u''^c\}\epsilon_{rsu}$, with Q, Q', Q'' denoting generic quark fields and r, s, u color indices.

III. PTG OPERATORS THAT DO NOT CONTAIN RIGHT-HANDED NEUTRINO FIELDS

We will consider separately operators that contain right-handed neutrinos in Sec. V below; here we will discuss the leading effects of dimension-7 operators containing only SM fields and which can be generated at tree level. There are 20 such operators:

$$\begin{aligned}
&\mathcal{O}_1 = (\overline{\ell^c}\epsilon D^\mu \phi)(\ell \epsilon D_\mu \phi), && \mathcal{O}_2 = (\overline{e^c}\gamma^\mu N)(\phi \epsilon D_\mu \phi),\\
&\mathcal{O}_3 = (\overline{\ell^c}\epsilon D_\mu \ell)(\phi \epsilon D^\mu \phi), && \mathcal{O}_4 = \overline{N^c}(D_\mu \phi \epsilon D^\mu \ell),\\
&\mathcal{O}_5 = (\overline{N^c}\ell)\epsilon(\bar{e}\ell), && \mathcal{O}_6 = (\overline{N^c}N)|\phi|^2,\\
&\mathcal{O}_7 = [\overline{N^c}\sigma^{\mu\nu}(\phi \epsilon \mathbf{W}_{\mu\nu}\ell)], && \mathcal{O}_8 = (\overline{N^c}\sigma^{\mu\nu}N)B_{\mu\nu},\\
&\mathcal{O}_9 = (\bar{d}q)\epsilon(\overline{N^c}\ell), && \mathcal{O}_{10} = [(\overline{q^c}\phi)\epsilon\ell)(\bar{d}\ell),\\
&\mathcal{O}_{11} = (\overline{N^c}q)\epsilon(\bar{d}\ell), && \mathcal{O}_{12} = (\overline{\ell^c}\epsilon q)(\bar{d}N),\\
&\mathcal{O}_{13} = (\bar{d}N)(u^T C e), && \mathcal{O}_{14} = (\overline{N^c}\ell)(\bar{q}u),\\
&\mathcal{O}_{15} = (\bar{u}d^c)(\bar{d}N), && \mathcal{O}_{16} = [\overline{q^c}(\phi^\dagger q)]\epsilon(\bar{\ell}d),\\
&\mathcal{O}_{17} = (\overline{q^c}\epsilon q)(\bar{N}d), && \mathcal{O}_{18} = (\bar{d}d^c)(\bar{d}E),\\
&\mathcal{O}_{19} = (\bar{e}\phi^\dagger q)(\overline{d^c}d), && \mathcal{O}_{20} = (\bar{u}N)(\bar{d}d^c).
\end{aligned} \qquad (13)$$

This list coincides with the one previously presented in the literature [15].

Using the results of Appendix A, it is a straightforward exercise to determine the types of new physics that can generate those operators at tree level.

A. Constraints on PTG operators without right-handed neutrinos

There are a variety of existing data that can be used to constrain the scale of new physics responsible for the operators being considered here. In this section, we provide limits for the PTG operators listed in Eq. (13); in obtaining the numbers below, we assumed no deviations from the SM and took 3σ intervals. Though there are processes that can receive contributions from more than one operator, we will provide limits for the most conservative case where there are no interference effects or cancellations (if this is

relaxed, the restrictions can be much weaker); we also assume that the gauge bosons are universally coupled (so they always appear multiplied by the corresponding gauge coupling). All limits below are on $\tilde{\Lambda} = \Lambda/f^{1/3}$ and translate into limits on the new physics scale with the additional naturality assumption $f \sim 1$ (for weakly coupled heavy physics). We also provide separately the limits derived from neutrinoless double-beta decay experiments (for a recent review, see Ref. [27]) to illustrate the importance of this high-precision measurement.

(1) There are no published limits on $\tilde{\Lambda}$ for $\mathcal{O}_1$ from collider or gauge-boson decay data. This operator, however, contributes to neutrinoless double-beta decay [28] that gives the limit $\tilde{\Lambda} > 7.5$ TeV.
(2) The strictest limits on $\tilde{\Lambda}$ for $\mathcal{O}_{2,3,4,5}$ from gauge boson decays [29] are $\mathcal{O}_2$: 400 GeV ($W \to \ell\nu$); $\mathcal{O}_3$: 35 GeV ($W \to \ell\nu$); $\mathcal{O}_4$: 92 GeV ($Z \to \nu\nu$); and $\mathcal{O}_5$: 182 GeV ($ee \to \nu\nu$), assuming the same error as in the invisible decay width of the Z. The best limits on $\mathcal{O}_{2,3,4}$ are derived from their contribution to neutrinoless double-beta decay: $\mathcal{O}_2$: 106 TeV; $\mathcal{O}_{3,4}$: 7.5 TeV.
(3) The strictest limits on $\tilde{\Lambda}$ for $\mathcal{O}_6$ from neutrino mass constraints is 770 TeV [29]. The limit from neutrinoless double-beta decay is significantly stronger: $\tilde{\Lambda} > 2,200$ TeV.
(4) The strictest limits on $\tilde{\Lambda}$ for $\mathcal{O}_{7,8}$ are obtained from limits on red-giant cooling [30] generated by plasmon decay $\gamma \to \nu\nu$, which is mediated by these operators. Using the results in Ref. [20], we find $\mathcal{O}_7$: 33 TeV; and $\mathcal{O}_8$:47 TeV. The neutrinoless double-beta decay on $\mathcal{O}_7$ is weaker: $\tilde{\Lambda} > 7.5$ TeV.
(5) The limit on $\tilde{\Lambda}$ for $\mathcal{O}_{9,10,11,12,13,14}$ obtained from $\pi \to e\nu$ decay is 2.1 TeV [29]. The limit derived from neutrinoless double-beta decay is stronger: $\tilde{\Lambda} > 137$ TeV.
(6) The strictest constraint on $\tilde{\Lambda}$ for the baryon-number-violating operators $\mathcal{O}_{15,16,17}$ is obtained from the limit on $n \to \pi\nu$ decay and given as 1.9×10^8 TeV [29].
(7) The strictest limits on $\tilde{\Lambda}$ for the baryon-number-violating operators $\mathcal{O}_{18,19,20}$ are obtained from neutron decay: $\mathcal{O}_{18,19}$: 9.6×10^7 TeV$(n \to eK)$; and $\mathcal{O}_{20}$: 1.5×10^8 TeV$(n \to \nu K^0_S)$ [29].

It is worth noting that any such new physics that generates the operators $\mathcal{O}_{1,3,4}$ at tree level necessarily generates the dimension-5 operator $\mathcal{O}^{(5)} = \overline{N^c}N$ also at tree level [28], and the limits on Λ derived from the latter are much stronger: 10^{11} TeV [assuming $O(1)$ couplings].

As can be seen from the above results, the PTG operators in Eq. (13) without right-handed neutrinos but containing quarks are highly constrained from various precision measurements and astrophysical observations. These results rely heavily on the assumption that there are no interference effects among the various operator contributions—when these are present, the above limits can be significantly degraded. (Such cancellations may result from some unknown symmetry and are not necessarily from fine-tuning.) Because of this, probing the individual operator effects (see the following section for an example) is of importance in mapping potential NP contributions, even though this usually provides weaker limits.

B. Neutrino Majorana masses

The PTG operators $\mathcal{O}_{1-14}$ in Eq. (13) generate neutrino Majorana masses through radiative corrections [28], which have the generic form $m_{\nu\text{–Maj}} \sim v^2/(16\pi^2\Lambda)$, multiplied in some cases by a SM Yukawa coupling. A detailed phenomenological investigation of the consequences of these effects is best done within the context of specific models, since correlations between effective operator contributions can be important (see e.g. Ref. [31]); for example, the operator coefficients for $\mathcal{O}_{1,3,4,6-8}$ may contain Yukawa couplings that mix heavy and light fermions, whose impact cannot be gauged within this effective approach. We will then restrict ourselves to displaying the generic expressions obtained using straightforward estimates:

Operator(s)	$m_{\nu\text{-Maj}}$estimate
$\mathcal{O}_{1,3,4,6-8}$	$v^2/(16\pi^2\Lambda)$
$\mathcal{O}_{2,5}$	$vm_e/(16\pi^2\Lambda)$
$\mathcal{O}_{9-12}$	$vm_d/(16\pi^2\Lambda)$
$\mathcal{O}_{14}$	$vm_u/(16\pi^2\Lambda)$

, (14)

where $m_{e,d,u}$ denote the masses of light charged leptons, down quarks and up quarks, respectively; $\mathcal{O}_{13}$ contributes only at two loops, and $\mathcal{O}_{15-20}$, being baryon-number violating, generate contributions only through graphs quadratic in the effective operators.

A measure of care should be exerted in obtaining the contributions from $\mathcal{O}_{1,3,4,6-8}$: for example, after spontaneous symmetry breaking and in unitary gauge,

$$\mathcal{O}_1 \supset \frac{1}{2}[(\partial H)^2 - m_Z^2 Z^2](\overline{\nu_L^c}\nu_L), \tag{15}$$

which generates two contributions to $m_{\nu\text{-Maj}}$, one from a Higgs (H) loop and another a Z. Each loop gives $\Lambda/(16\pi^2)$ to leading order, but they cancel, leaving only the subleading contribution listed above. This cancellation is not accidental: an examination of the operators shows that, absent the spontaneous breaking of the SM gauge symmetry, they do not generate one-loop contributions to $m_{\nu\text{–Maj}}$.

For $m_{\nu\text{–Maj}} \sim 0.1$ eV, we obtain from Eq. (14) $\Lambda \sim 8 \times 10^3$–$4 \times 10^9$ TeV depending on the operator used, and assuming all operator coefficients are $O(1)$.

IV. EXAMPLE OF AN LHC EFFECT

Consider the PTG operators $\mathcal{O}_1 = (\overline{\ell^c}\epsilon D^\mu\phi)(\ell\epsilon D_\mu\phi)$ and $\mathcal{O}_3 = (\overline{\ell^c}\epsilon D_\mu\ell)(\phi\epsilon D^\mu\phi)$ from Eq. (13). It is easy to see that, in unitary gauge, they both contain the same

lepton-number-violating vertex involving two W gauge bosons and two left-handed charged leptons:

$$(\overline{\ell^c}\epsilon D_\mu \ell)(\phi \epsilon D^\mu \phi),$$

$$(\overline{\ell^c}\epsilon D^\mu \phi)(\ell \epsilon D_\mu \phi) \supset m_W^2\left(1+\frac{h}{v}\right)^2 W^{+2}(e_L^T C e_L). \quad (16)$$

[No other operator in Eq. (13) contains this vertex.] Despite their both containing the vertex in Eq. (16), $\mathcal{O}_{1,3}$ are generated at tree level by different types of heavy physics (see Appendix A); this will be of use in understanding the types of NP that can be probed through Eq. (16); see Sec. IV E.

Below, we will consider the effects of the right-hand side in Eq. (16) in the production of same-sign dileptons at the LHC, and determine the constraints on the scale of new physics Λ that can be derived from existing data. It should be noted that $\mathcal{O}_{1,3}$ also contain other lepton-number-violating vertices in addition to the one in Eq. (16): $\mathcal{O}_1 \supset W\nu e, WZ\nu e, WA\nu e, WW\nu\nu$ and $\mathcal{O}_3 \supset ZZ\nu\nu, WZ\nu e$, plus others involving the Higgs field; these will contribute to a variety of other reactions from which independent constraints on Λ can be derived. Note, however, that such vertices involve one or more neutrinos and/or Higgs fields, and because of this, the corresponding constraints will be weaker. It is for this reason that we concentrate on the term containing two charged leptons; the constraints on Λ using this term of course apply to all the vertices contained in $\mathcal{O}_{1,3}$.

In the following, we will define

$$\mathcal{O}_{\ell\ell} = f_1\mathcal{O}_1 + f_3\mathcal{O}_3 \quad (17)$$

and consider separately the same-sign dilepton signal associated with two jets and the hadronically quiet trilepton events at the Large Hadron Collider (LHC) generated by this operator.

A. Same-sign dilepton signal at the LHC

$\mathcal{O}_{\ell\ell}$ in Eq. (17) will produce a dilepton signal $pp \to \ell\ell jj$ at LHC; where $\ell = e, \mu$ have the *same* sign, and the j denote light-quark jets (after tagging efficiencies are included, the number of τ-lepton events is too small to be of interest). In Fig. 1, we show the dominant Feynman diagrams that contribute to the $\ell\ell jj$ final state generated by this operator; these can be separated into s-channel reactions and t-channel reactions; we will see that the latter dominate over the former. In the s-channel contributions (diagrams a, d in the figure), one W in the vertex Eq. (16) couples to the quarks in the colliding protons, while the other couples to the light jets in the final state; in the t-channel processes (diagrams b, c, e, f) each W couples to an incoming and an outgoing quark.

As $\mathcal{O}_{\ell\ell}$ is of dimension 7, its coefficient contains a Λ^3 suppression factor that will prevent probing new physics above the TeV region, as we will shortly demonstrate. Even with this limitation, we will argue that the constraints

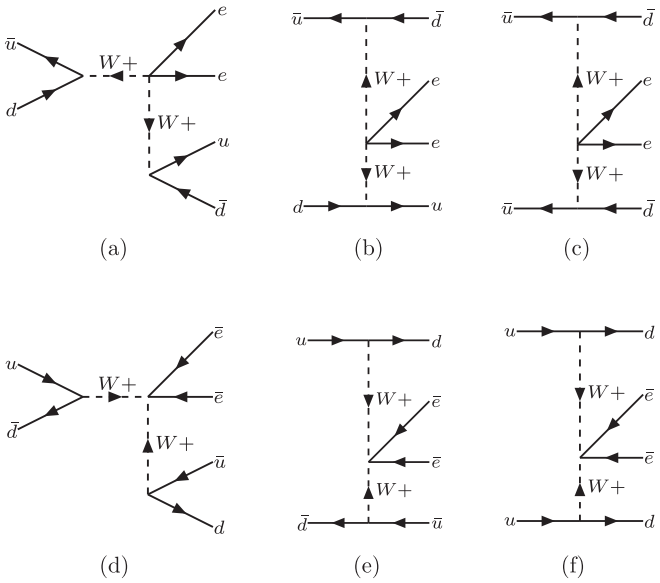

FIG. 1. Leading Feynman diagrams that contribute to $pp \to \ell\ell jj$ at the LHC; the $eeWW$ vertex [Eq. (16)] is generated by $\mathcal{O}_{\ell\ell}$ in Eq. (17).

obtained are of interest. In the following, we will assume the effective operator coefficients are $O(1)$; if this is not the case, the limits obtained apply to the scale $\tilde{\Lambda}$ introduced in Sec. III A.

We note here that such a lepton-number-violating signal ($eeu\bar{d}, ee\bar{d}\,\bar{d}, \bar{e}\,\bar{e}\,\bar{u}\,d, \bar{e}\,\bar{e}\,dd$) cannot be exclusively produced by SM, which conserves lepton number. Since the amplitude contains $1/\Lambda^3$ from $\mathcal{O}_{\ell\ell}$, the signal cross section will be proportional to $1/\Lambda^6$, so that

$$\sigma^{(\text{signal})}_{\ell\ell jj}(\Lambda') = \left(\frac{\Lambda}{\Lambda'}\right)^6 \sigma^{(\text{signal})}_{\ell\ell jj}(\Lambda). \quad (18)$$

Thus, we can compute the cross section at a convenient value of Λ and use this scaling property to obtain $\sigma_{\ell\ell jj}$ for any other scale. In the following, we evaluate first $\sigma_{\ell\ell jj}$ for $\Lambda = 100$ GeV at the LHC for 14 TeV and 8 TeV CM energies (see Table III). We obtained these results using the `Calchep 3.6.14` [32] event generator to calculate the hard cross sections, and we chose the CTEQ6L parton distribution function [33] with the invariant mass of the two incoming quarks as the renormalization and factorization scales. There is a variation of up to ~15% in the cross section when the parton distribution function and the renormalization and factorization scales are varied, which can presumably be addressed by a next-to-leading-order calculation; this effort, however, lies beyond the scope of this investigation. We also imposed the following basic cuts:

$$C1:\ p_{T(\ell,j)} > 15\ \text{GeV}, \qquad |\eta_\ell| < 2.5, \quad (19)$$

where $p_{T(\ell,j)}$ denotes the lepton and jet transverse momenta, and η_ℓ denotes the lepton pseudorapidity. It is worth noting

TABLE III. Total cross section for $\ell\ell jj$ production, and of the leading contributing subprocesses at the LHC with $E_{\rm CM} = 14$ and 8 TeV generated by the operator $\mathcal{O}_{\ell\ell}$. The last column indicates the effects of the cuts in Eq. (19). We use $\Lambda = 100$ GeV (see text).

$E_{\rm CM} = 14$ TeV			
Process	Leading subprocesses	σ (pb)	σ after C_1 (pb)
$pp \to eeqq$	$dd \to eeuu$	0.142	0.118
	$\bar{u}d \to ee\bar{d}u$	0.039	0.038
	$sd \to eeuc$	0.024	0.020
	$dd \to eeuc$	0.015	0.014
	Total[a]	0.253	0.215
$pp \to \bar{e}\bar{e}qq$	$uu \to \bar{e}\,\bar{e}\,dd$	0.942	0.784
	$u\bar{d} \to \bar{e}\,\bar{e}\,d\bar{u}$	0.121	0.100
	$uu \to \bar{e}\,\bar{e}\,ds$	0.097	0.082
	$u\bar{s} \to \bar{e}\,\bar{e}\,d\bar{c}$	0.064	0.052
	Total	1.300	1.080
$pp \to \ell\ell qq$	Sum of all contributions for $\ell = e, \mu$	3.106	2.590

$E_{\rm CM} = 8$ TeV			
Process	Subprocesses	σ (pb)	σ after C_1 (pb)
$pp \to eeqq$	$dd \to eeuu$	0.016	0.012
	$\bar{u}d \to ee\bar{d}u$	0.004	0.003
	$ds \to eeuc$	0.002	0.002
	$dd \to eeuc$	0.002	0.001
	Total	0.028	0.021
$pp \to \bar{e}\,\bar{e}\,qq$	$uu \to \bar{e}\,\bar{e}\,dd$	0.102	0.084
	$u\bar{d} \to \bar{e}\,\bar{e}\,d\bar{u}$	0.013	0.010
	$uu \to \bar{e}\,\bar{e}\,ds$	0.010	0.009
	$u\bar{s} \to \bar{e}\,\bar{e}\,d\bar{c}$	0.006	0.005
	Total	0.140	0.115
$pp \to \ell\ell qq$	Sum of all contributions for $\ell = e, \mu$	0.336	0.273

[a]Totals refer to the sum of all contributions, not only the leading ones.

that there will be a difference in the production cross sections for positively and negatively charged same-sign dileptons, which is due to the difference in the u- and d-parton distributions in the proton; there would be no such difference in a $p\bar{p}$ machine.

All calculations were made in the unitary gauge (again we emphasize that the choice of $\Lambda = 100$ GeV is made for calculational ease, and not with the assumption that there is new physics lurking at 0.1 TeV); the $1/\Lambda^6$ behavior of $\sigma_{\ell\ell jj}$ as Λ changes is presented in Fig. 2. For example, we see that for $\Lambda = 500$ GeV, $\sigma_{\ell\ell jj} = 0.165$ fb at 14 TeV CM energy [after the cuts C1 in Eq. (19) are imposed]. This corresponds to 16 events for an integrated luminosity of 100 fb^{-1} (consistent with the expectations for "run 2" at the LHC [34,35]); this would increase to 497 events for the proposed high-luminosity upgrade [36] with a projected integrated luminosity of 3000 fb^{-1}. For 7 and 8 TeV CM energies and $\Lambda = 500$ GeV, the cross section drops to 0.011 fb and 0.017 fb, respectively, and has no observable effects.

The discovery limit, however, depends on the SM background estimate for the $\ell\ell jj$ signal, which we discuss below. We will use these results to obtain the current limits on Λ derived from the 8 TeV LHC data, and to derive the expected sensitivity that will be reached when the CM energy is increased to 14 TeV.

1. SM background for same-sign dilepton signal at the LHC

The most significant background contribution to our process is generated by SM $t\bar{t}$ production, with marginal contributions from $t\bar{t}W$, $t\bar{t}Z$ and diboson production. For the $t\bar{t}$ background calculation, we take $m_{\rm top} = 173.34$ GeV [37] and use the `Pythia 6.4` [38] event generator at tree level, which we multiply the by the appropriate K factor[4] to obtain the NLO + NLL cross section at the LHC [39–41]. This K factor is very significant—for example, the `Pythia` $t\bar{t}$ production cross section is 386.8 pb at 14 TeV, while the NNLO prediction is between 805 and 898 pb (incorporating the jet energy scale and parton distribution function uncertainties); we use the average value of 851.5 pb that gives a $K = 2.2$ factor. For $E_{\rm CM} = 8$ TeV, the `Pythia` prediction is 94 pb, while the measured value [40] in the dilepton and lepton + jet channels is 161.9 pb (there are variations in this number depending on the channel used), so that we use $K = 1.7$ in this case.

In our analysis, we try to mimic the experimental reconstruction for leptons and jets within `Pythia` by imposing the following requirements:

(1) *Leptons* (ℓ) are identified as electrons and muons with transverse momentum $p_T > 10$ GeV and rapidity $|\eta| < 2.5$. Two leptons with pseudorapidities η and $\eta + \Delta\eta$, and azimuthal angles ϕ and $\phi + \Delta\phi$, will be considered isolated if $\Delta R = \sqrt{(\Delta\eta)^2 + (\Delta\phi)^2} \geq 0.2$. A lepton and a jet will be isolated if $\Delta R \geq 0.4$ and if the $\Delta R \leq 0.2$ cone contains less than 10 GeV of transverse energy from low-E_T hadron activity.

(2) *Jets* (j) are formed with all the final-state particles after removing the isolated leptons from the list with `PYCELL`, a built-in cluster routine within `Pythia`. The detector is assumed to span the pseudorapidity range $|\eta| \leq 5$ and to be segmented in 100-η and 64-ϕ bins. The minimum transverse energy E_T of each cell is taken as 0.5 GeV, while we require $E_T \geq 2$ GeV for a cell to act as a jet initiator. All the partons within $\Delta R = 0.4$ from the jet initiator cell are included in the formation of the jet, and we

[4]The K factor is used to correct the tree-level cross sections used by `Pythia` so they match the NLO + NLL predictions or the experimental data; these (mostly QCD) corrections can be significant, as in the case in $t\bar{t}$ production of interest here.

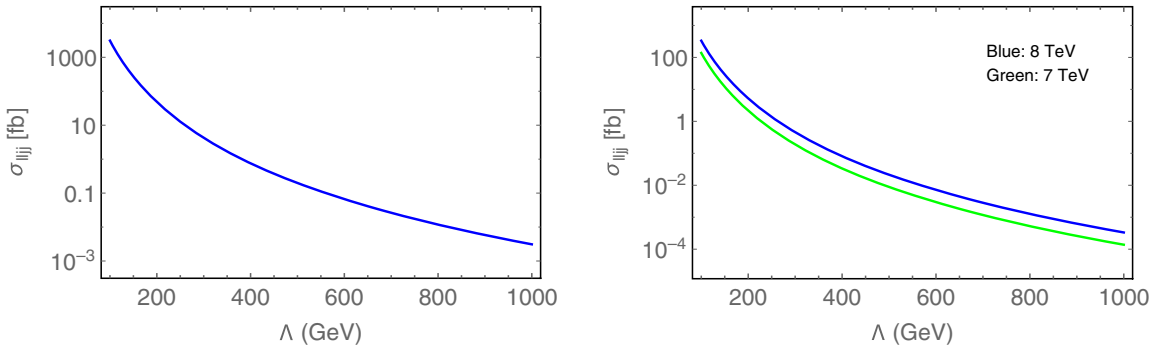

FIG. 2. Production cross section for two same-sign leptons and two jets ($\ell\ell jj$) as a function of Λ (GeV) at LHC with $E_{\rm CM} = 14$ TeV (left) and 7,8 TeV (right) in green and blue, respectively.

require $E_T \geq 20$ GeV for a cell group to be considered a jet.

We now define the invariant lepton mass $M_{\ell\ell}$ and the transverse event mass H_T by

$$M^2_{\ell\ell} = 2|\mathbf{p_1}||\mathbf{p_2}|(1-\cos\theta), \qquad H_T = \sum_{\ell,j}|\mathbf{p}_\perp|, \quad (20)$$

where θ is the relative angle of the lepton momenta $\mathbf{p_1}$ and $\mathbf{p_2}$, and we neglect the lepton masses; $\mathbf{p}_\perp$ denotes the corresponding momenta perpendicular to the beam. The $M_{\ell\ell}$ and H_T distributions are plotted in Fig. 3 for the signal subprocesses $\bar{e}\,\bar{e}\,jj$ (lilac) and $eejj$ (green). We see that the signal distribution from $\bar{e}\,\bar{e}\,jj$ peaks at values $M_{\ell\ell} \sim$ 1–2 TeV (this property is independent of Λ), while the SM background is already much suppressed at $M_{\ell\ell} \simeq$ 2 TeV (see Fig. 5). Also from Fig. 3, we find that the corresponding H_T distribution for signal events peaks at 500–1000 GeV, while the background is already negligible at 1 TeV (see Fig. 6).

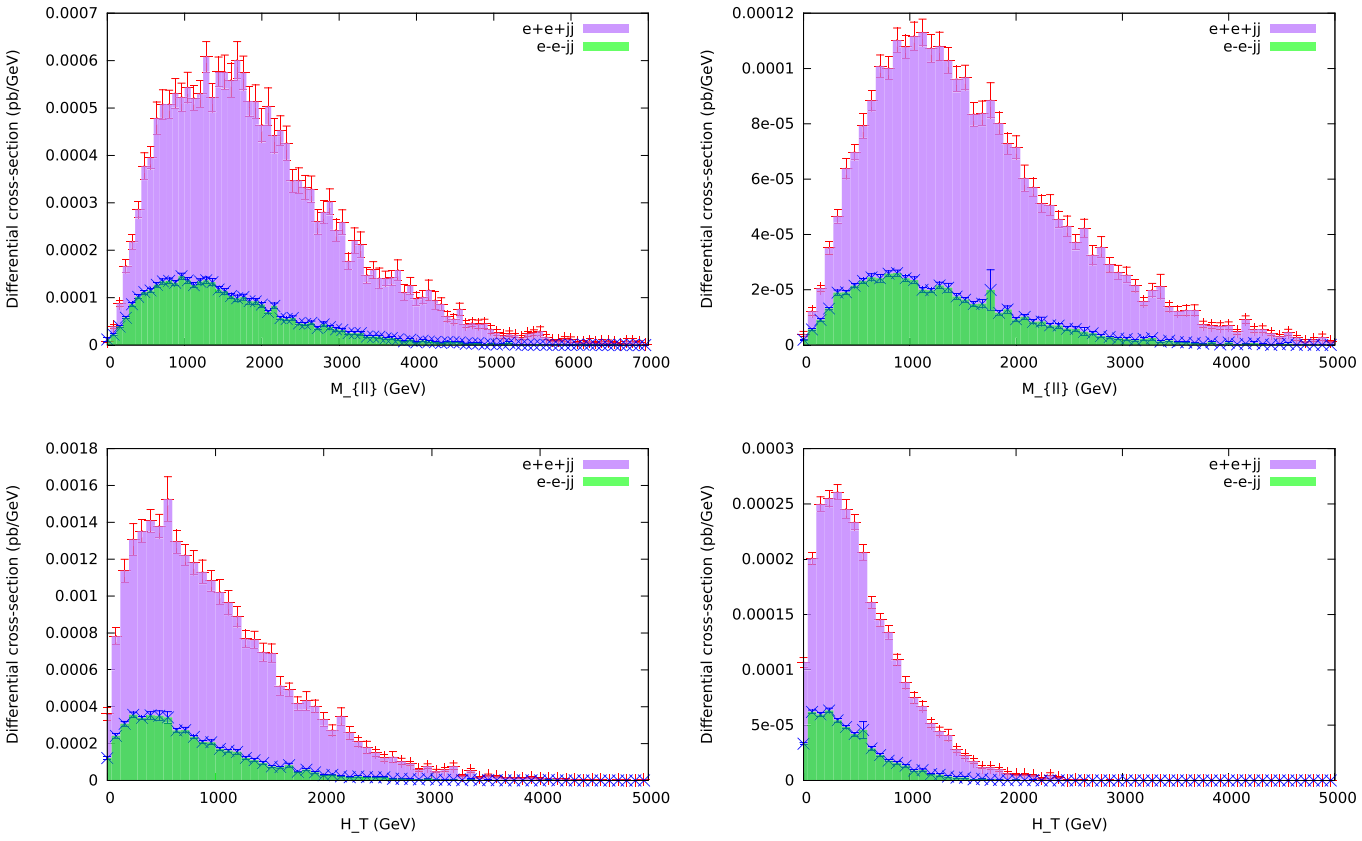

FIG. 3. Distributions of the invariant mass of leptons $M_{\ell\ell}$ (top) and transverse mass H_T (bottom), for the $\ell\ell jj$ signal events at LHC with $E_{\rm cm} = 14$ TeV (left) and $E_{\rm cm} = 8$ TeV (right). We took $\Lambda = 100$ GeV [see text and Eq. (18)]. Subprocesses $\bar{e}\,\bar{e}\,jj$ (red dots and lilac histograms) and $eejj$ (blue crosses and green histograms) are shown separately.

TABLE IV. Dominant SM background cross section from $t\bar{t}$ production (in pb) for same-sign dilepton events at $E_{\rm cm} = 14, 8$ TeV including muons, antimuons, electrons or positrons. The fourth (last) column cross sections are obtained by requiring $E_{\not t} = 0$ ($E_{\not t} \leq 15$ GeV); see text. The cross sections are obtained after multiplying by the appropriate K factor: 2.20 for 14 TeV and 1.7 for 8 TeV.

$t\bar{t}$ Production at LHC	$\sigma^{(tt)}_{\ell\ell}$	$\sigma^{(tt)}_{\ell\ell jj}$	$\sigma^{(tt)}_{\ell\ell jj-0}$	$\sigma^{(tt)}_{\ell\ell jj-15}$
$E_{\rm CM} = 14$ TeV	0.47	0.145	$\leq 0.85 \times 10^{-3}$	0.0077
$E_{\rm CM} = 8$ TeV	0.089	0.0282	$\leq 0.162 \times 10^{-3}$	0.001

The signal events consist of leptons plus jets and do not involve particles like neutrinos that are not detected at the LHC, while the background events that closely mimic the chosen signal do produce neutrinos which pass through the detector undetected. Therefore, signal events will be characterized by having zero missing transverse to the beam, while any nonzero measurement of the missing transverse energy

$$E_{\not t} = \left| \sum_{\ell, j} \mathbf{p}_\perp \right| \tag{21}$$

(where the vector sum is over all visible leptons and jets, and $\mathbf{p}_\perp$ denotes the corresponding momenta perpendicular to the beam) will indicate the presence of particles like neutrinos in the final state, and will correspond to a background event.[5] We will then require $E_{\not t} \leq 15$ GeV, in addition to $C1$ in Eq. (19). The usefulness of this cut can be gauged by comparing the cross sections associated with $t\bar{t}$ production listed in Table IV: $\sigma_{\ell\ell}$ denotes the dilepton production cross section (two same-sign leptons plus anything); $\sigma_{\ell\ell jj}$ the dilepton-plus-two-jet cross section, when both jets have transverse momentum $p_T^{(j)} \geq 25$ GeV; $\sigma_{\ell\ell jj-0}$ the dilepton-plus-two-jet cross section[6] with zero missing energy ($E_{\not t} = 0$) and $p_T^{(j)} \geq 25$ GeV, and for which we obtain less than 1 event in our simulations. Finally, $\sigma_{\ell\ell jj-15}$ the dilepton-plus-two-jet cross section with missing energy $E_{\not t} \leq 15$ GeV and $p_T^{(j)} \geq 25$ GeV. We will use these last two quantities to derive a bound on Λ (for $E_{\rm CM} = 8$ TeV) and determine the expected sensitivity for $E_{\rm CM} = 14$ TeV.

The missing energy $E_{\not t}$ distribution for the SM background (Fig. 4) shows that there is a very large number of $\ell\ell jj$ events with $E_{\not t} < 100$ GeV, and that this is drastically reduced to a vanishingly small number when the cut $E_{\not t} < 15$ GeV is imposed, as also shown in Table IV. This clearly indicates that with such a selection criteria, the signal events are retained (as ideally they are characterized by having zero missing energy), while the background can be reduced significantly, allowing for a much improved discovery limit. In addition, the invariant lepton mass $M_{\ell\ell}$ (Fig. 5) and transverse event mass H_T (Fig. 6) distributions show a characteristic difference between signal and background. For example, the $M_{\ell\ell}$ distribution for signal (upper panel of Fig. 3) peaks at $M_{\ell\ell} \sim 800$ GeV, while the one for background (Fig. 5) peaks between $M_{\ell\ell} \sim 0$ and 10 GeV, which can be also used for distinguishing between the contributions from new physics and the SM background.

B. Bound on Λ from LHC data

The LHC has not seen even a 1σ excess from the background events, so assuming Gaussian statistics,

$$S/\sqrt{B} \leq 1,$$

where S and B denote the number of signal and background events, respectively. In terms of the luminosity L and the corresponding cross sections, $S = \sigma_{\rm signal} L, B = \sigma_{\rm back} L$, where L is integrated luminosity. To date CMS has analyzed LHC data for same-sign dileptons for $L = 19.5$ fb^{-1} at 8 TeV [42]; the background cross section corresponds to $\sigma_{\rm back} = \sigma^{(tt)}_{\ell\ell jj-15} = 1$ fb in Table IV, and we then find

$$\sigma_{\rm signal} \leq 0.224 \text{ fb}.$$

This in turn puts the bound on the new physics scale: we know that $\sigma_{\rm signal} = 273$ fb (after cuts) when $\Lambda = 100$ GeV (see Table III), and that the signal cross section scales as $1/\Lambda^6$ [see Eq. (18)]. It follows that

$$\Lambda \geq \left(\frac{273 \text{ fb}}{0.224 \text{ fb}} \right)^{1/6} \times 100 \text{ GeV} = 327 \text{ GeV}. \tag{22}$$

C. Discovery limit for Λ for $\mathcal{O}_{ee}$ at the LHC

We will follow the same approach to evaluate the discovery limit at the 14 TeV LHC, requiring now a 3σ excess over the background:

$$\sigma_{\rm signal} \geq 3\sqrt{\frac{\sigma_{\rm back}}{L}}.$$

From Table IV, we find $\sigma_B = \sigma^{(tt)}_{\ell\ell jj-15} = 7.7$ fb, while from Table III we find $\sigma_{\rm signal} = 2590$ fb (after cuts) when the new physics scale $\Lambda = 100$ GeV. Using again the simple

[5] Of course, real detectors miss particles, and may misidentify one type of event for the other.

[6] Our simulations generated no $t\bar{t}$ events with $E_{\not t} = 0$; the corresponding limits for $\sigma_{\ell\ell jj-0}$ are obtained as follows: If a simulation with N events produces less than 1 event for a process with cross section σ, then $L\sigma/N < 1$, where L is the luminosity, so that $\sigma < N/L$. The numbers presented were obtained using $L = 10$ fb^{-1} at 8 TeV and $L = 1$ fb^{-1} at 14 TeV.

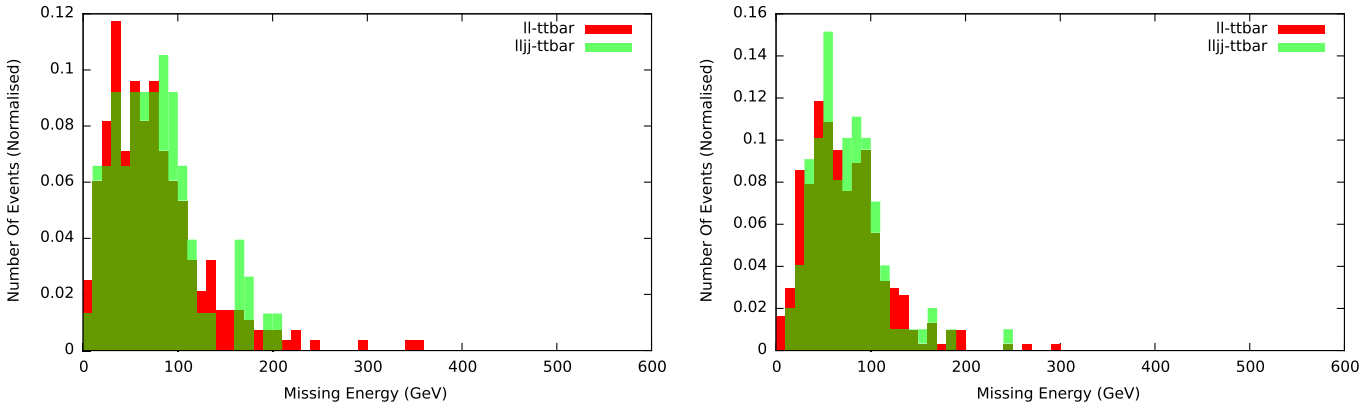

FIG. 4. $E_{\not t}$ distribution for $t\bar{t}$ events at the LHC with two leptons (light green) and two leptons and two jets (red); dark green regions correspond to the overlap of the two distributions. Left: $E_{\rm cm} = 14$ TeV. Right: $E_{\rm cm} = 8$ TeV.

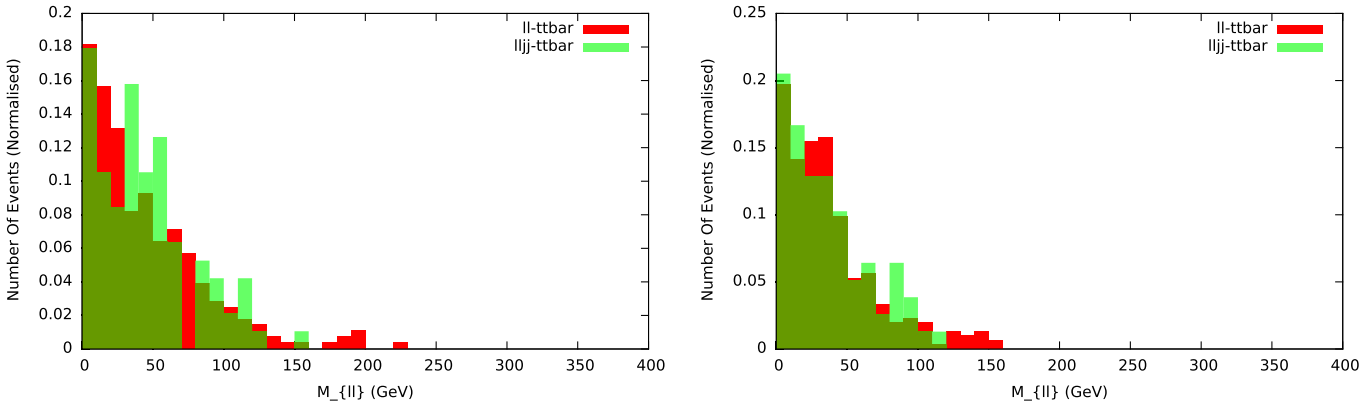

FIG. 5. $M_{\ell\ell}$ distribution of the leptons for $t\bar{t}$ events at LHC. The distributions for $\ell\ell$ and $\ell\ell 2j$ events are shown in red and light green, respectively (dark green regions correspond to the overlap of the two distributions). Left: $E_{\rm cm} = 14$ TeV. Right: $E_{\rm cm} = 8$ TeV.

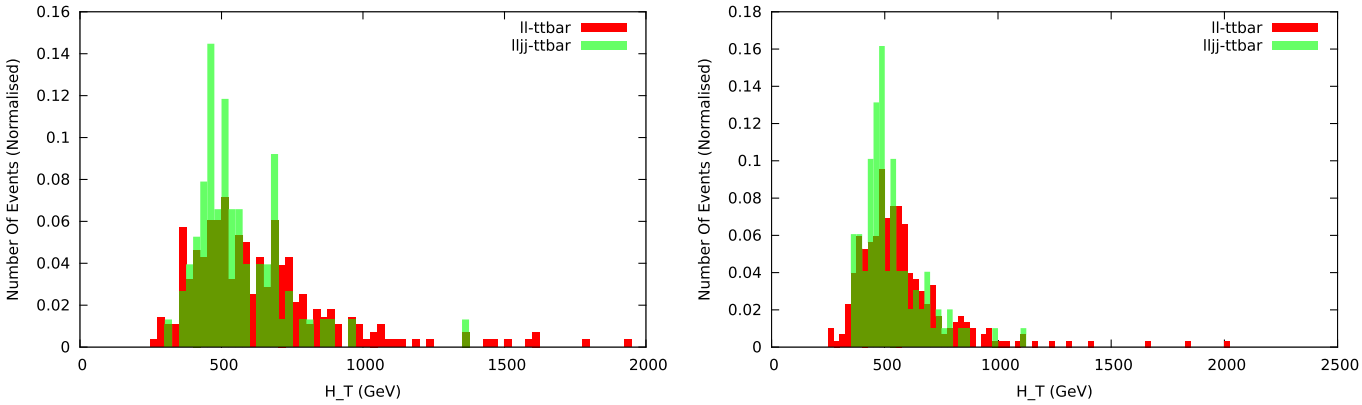

FIG. 6. H_T for $t\bar{t}$ events at LHC. The distributions for $\ell\ell$ and $\ell\ell 2j$ events are shown in red and light green, respectively (dark green regions correspond to the overlap of the two distributions). Left: $E_{\rm cm} = 14$ TeV. Right: $E_{\rm cm} = 8$ TeV.

scaling of the signal cross section with Λ [see Eq. (18)], we find

$$\Lambda \leq 382 \text{ GeV}(L = 100 \text{ fb}^{-1}, E_{\not t} \leq 15 \text{ GeV}), \quad (23)$$

for an integrated luminosity $L = 100$ fb^{-1}.

If we use a stronger missing energy cut, the limit improves. If we require no missing transverse energy, then the background cross section drops to $\sigma^{(t\bar{t})}_{\ell\ell jj-0} = \sigma_{\rm back} = 0.85$ fb (see Table IV) so that, for the same luminosity,

$$\Lambda \leq 459 \text{ GeV}(L = 100 \text{ fb}^{-1}, E_{\not t} = 0 \text{ GeV}). \quad (24)$$

TABLE V. Cross sections for the hadronically quiet trilepton signal at the LHC with $E_{\rm cm} = 14$ TeV. σ_1 is obtained by imposing the cut $C1$ [cf. Eq. (19)], and σ_2 by both imposing $C1$ and demanding $|M_{e\bar{e}} - M_z| > 15$ GeV.

$p, p \to \ell, \ell, \ell, \nu_\ell$	σ (fb)	σ_1 (fb)	σ_2 (fb)
$p, p \to \bar{e}, \bar{e}, e, \bar{\nu_e}$	1.2	0.70	0.695
$p, p \to e, e, \bar{e}, \nu_e$	0.44	0.39	0.385
Total (including μ)	3.28	2.18	2.16

D. Hadronically quiet trilepton at the LHC

The operator $\mathcal{O}_{\ell\ell}$ can also produce hadronically quiet trilepton events at the LHC, which is sometimes favored as a signal for new physics because of its clean signature and small SM backgrounds. We find, however, that for $\mathcal{O}_{\ell\ell}$ the total signal cross section is only 3.28 fb for $\Lambda = 100$ GeV (see Table V). This small value results from the relatively small branching ratio of the W boson into leptons and the absence of a t-channel diagram that generates an important contribution to the $\ell\ell jj$ final state (compare Figs. 7 and 1).

WZ production generates a significant background to the process being considered; in order to suppress it, we require that the invariant mass $M_{\ell\ell}$ between any opposite-sign leptons of the same flavor satisfy $|M_{\ell\ell} - M_z| > 15\,\text{GeV}$. Comparing the results in Tables V and VI, we see that by using the cuts, we are able to significantly reduce the background compared to the signal cross section of 2.16 fb for $\Lambda = 100\,\text{GeV}$. Following a procedure similar to the one we used in analyzing the same-sign dilepton events and using Eq. (18), we determine the sensitivity to Λ using this hadronically quiet trilepton channel; using a 3σ limit, we obtain

$$\Lambda \leq 130\ \text{GeV} \quad (E_{\not{T}} \leq 15\ \text{GeV}),$$
$$\Lambda \leq 140\ \text{GeV} \quad (E_{\not{T}} = 0\ \text{GeV}) \qquad (25)$$

for a luminosity of 100 fb^{-1}. As expected from the smaller cross section, these limits are weaker than the ones previously obtained.

E. Applicability of the effective field theory

The results above indicate that the reach on the new physics scale Λ lies in the $\simeq$500 GeV range for the same-sign dilepton signature generated by the operator(s) $\mathcal{O}_{\ell\ell}$ at the LHC with a 14 TeV CM energy. On the other hand, the dilepton invariant mass distribution (Fig. 3) peaks at $\sim$1 TeV, a significantly higher value. We must then investigate whether the effective theory approach is valid in the above processes. Specifically, within the paradigm we have adopted (that of a weakly coupled, renormalization and decoupling heavy physics), we must determine whether this implies that in the reactions under consideration one or more heavy particles carries momentum $\geq\Lambda$ (in which case they could be directly produced, and the effective approach would not be applicable). In order to investigate this, we display in Fig. 8 the types of heavy physics that could generate at tree level the vertex of interest (containing two charged leptons of the same sign, two W bosons of the same sign and two scalar isodoublets).

We see from Fig. 8 that there are two possible cases:

(1) When the heavy particles carry a momentum equal to the invariant dilepton mass, in which case the heavy particle is a boson isotriplet of unit hypercharge, or

(2) When the heavy particles carry a momentum equal to the lepton-W invariant mass, in which case the heavy particle Σ will be a heavy fermion isotriplet or isosinglet of zero hypercharge.

The comments above indicate that the effective theory would not be applicable in case 1. The situation for the fermions Σ (case 2), however, is different: we see from

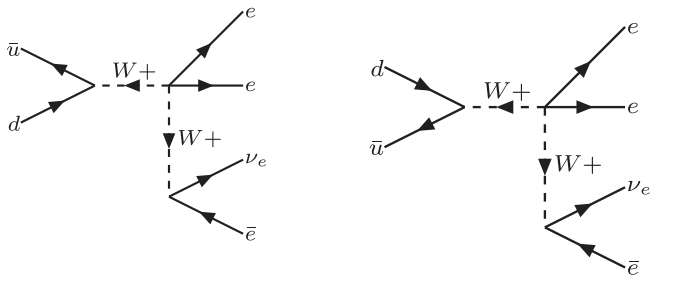

FIG. 7. Feynman diagrams generated by the operator $\mathcal{O}_{\ell\ell}$ and which contribute to the hadronically quiet trilepton channel $pp \to ee\bar{e}\nu_e$.

TABLE VI. Dominant SM background cross sections $\sigma_{\ell\ell\ell\ell}$ (in pb) generated by $t\bar{t}$ and WZ production for hadronically quiet trilepton events at $E_{\rm cm} = 14$ TeV including $\mu^\pm$ and $e^\pm$; the third column provides the numbers when the cut $|M_{\ell\ell} - M_z| > 15$ GeV is imposed on the events. The cross sections in the fourth and fifth columns are obtained by requiring $E_{\not{T}} = 0$ and $E_{\not{T}} \leq 15$ GeV, respectively (see text for details). The cross sections are obtained after multiplying by the appropriate K factor ($= 2.20$ for $t\bar{t}$).

SM Production at LHC	$\sigma_{\ell\ell\ell}$ (pb)	$\sigma_{\ell\ell\ell - M_{\ell\ell}}$ (pb)	$\sigma_{\ell\ell\ell - M_{\ell\ell} - 0}$ (fb)	$\sigma_{\ell\ell\ell - M_{\ell\ell} - 15}$ (fb)
$t\bar{t}$	0.99	0.031	$\leq$0.85	1.69
WZ	0.73	0.171	$\leq$0.058	0.46

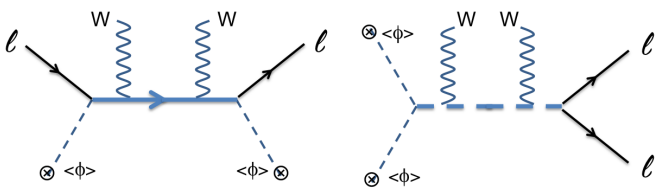

FIG. 8. Tree-level graphs that can generate the operators $\mathcal{O}_1$ and $\mathcal{O}_3$ by the exchange of a heavy fermion (left) or scalar (right), both isotriplets with unit hypercharge (denoted by the thick internal lines).

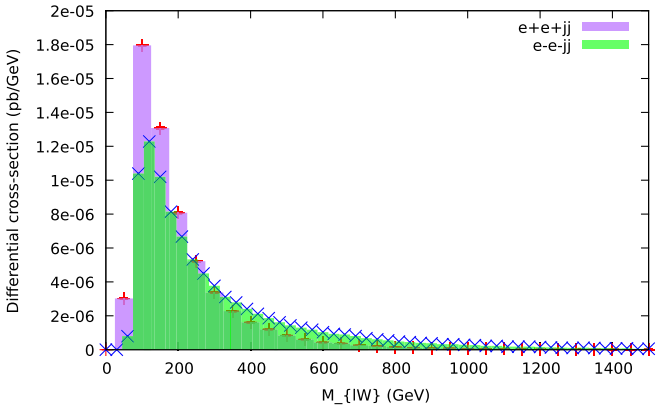

FIG. 9. Invariant mass distribution of the lepton with jets at LHC with $E_{\rm cm} = 14$ TeV. The red dots (on the lilac histogram) correspond to the $\bar{e}\,\bar{e}\,jj$ final state; while the blue crosses (on the green histogram) correspond to the $eejj$ final state (the green area corresponds to regions where these distributions overlap).

Fig. 9 that the lepton-W invariant mass peaks at $\lesssim$200 GeV, significantly below the limit on Λ. It follows that the limits we derive are applicable for the case where the new heavy physics corresponds to the same fermions Σ associated with type-III seesaw mechanisms [43] for neutrino mass generation (see Appendix A).[7]

Direct searches of such heavy fermion isotriplets Σ (using the full theory) at the 7 TeV LHC yield a bound $m_\Sigma \gtrsim 180$ GeV [44], with which our result $\Lambda \gtrsim 300$ GeV compares favorably. In addition, Ref. [45] presents an analysis where dimuon + jets data from the 8 TeV LHC are used to derive constraints on heavy Majorana neutrinos that can mix with the muon-neutrino (these correspond to the case where the Σ are isosinglets). The results exclude heavy fermion masses in the range 90–500 GeV, provided the mixing is $\geq$0.005 (for the low-mass limit) and $\geq$0.6 for the higher excluded mass; these constraints are then more stringent than the ones derived above for the case of large mixing. There are also several studies of the discovery potential of type-III seesaw fermions at the 14 TeV LHC through direct production [46–48] in lepton-rich final states, and though a comparative signature space analysis of the reach of direct production versus effective theory is beyond the scope of this paper, a benchmark point analysis in Ref. [46] suggests that the sensitivity to Λ obtained using effective field theory will be competitive with the one derived from direct searches.

V. CONSTRAINTS ON PTG OPERATORS WITH RIGHT-HANDED NEUTRINOS

In Sec. III A, we listed the operators that do not contain right-handed neutrinos and obtained the most stringent bounds on the scale of new physics. In this section, we do a similar study for operators that do contain right-handed neutrinos. The list of such operators and their expressions in unitary gauge can be found in Appendix B. Most of these operators contain vertices with three fields (see Table VII), one of which is a W, Z or H boson; the strictest limits on Λ are then derived from Z, W, H decays and neutrino magnetic moment, whenever kinematically allowed. When the right-handed neutrinos are too heavy for these decays to occur, the limits are weaker, as is the case for the operator $(\overline{\nu^c}\nu)|D\phi|^2$ that does not contain a three-legged vertex; we comment on this situation at the end of this section.

In the discussion below, we will assume that the right-handed neutrinos have a Majorana mass term of the form $\nu_R^T C M_\nu \nu_R$ that, for simplicity, we assume to be fully degenerate: $M_\nu = m_\nu \mathbb{1}$. In cases where the W, Z or H decays are allowed, the effects of mixing (generated by Dirac mass terms) will be small [49], and we will ignore them. As in Sec. III A, the limits on Λ obtained below are derived assuming that the operator coefficient is $O(1)$; if this is not the case, such limits apply to the scale $\tilde{\Lambda}$ defined in that section. We will also ignore the possibility of cancellations among various effective operator contributions.

A. Operators contributing to Z-invisible decay

There are two such operators (see Table VII):

$$\frac{1}{2}(\overline{\nu^c}\gamma^\mu N)(i\phi^\dagger \overleftrightarrow{D}_\mu \phi) \supset \frac{v^3}{2\sqrt{2}}\overline{\nu^c}\not{Z}P_L\nu,$$
$$|\phi|^2(\overline{\nu^c}\sigma^{\mu\nu}\nu)B_{\mu\nu} \supset -\frac{v^2 s_{\rm w}}{2}(\overline{\nu^c}\sigma^{\mu\nu}P_R\nu)Z_{\mu\nu} \quad (26)$$

(where $Z_{\mu\nu} = \partial_\mu Z_\nu - \partial_\nu Z_\mu$) that generate the following contributions to the invisible Z-decay width:

$$\frac{v^2 m_z}{\Lambda^3}\overline{\nu^c}\not{Z}P_R\nu:\ \Gamma_{Z1}(Z\to\nu_R\nu_R) = \frac{1}{96\pi}\left(\frac{v^2}{\Lambda^3}\right)^2(m_z^2-m_\nu^2)\sqrt{m_z^2-4m_\nu^2},$$
$$\frac{v m_z}{\Lambda^3}(\overline{\nu^c}\sigma^{\mu\nu}P_R\nu)Z_{\mu\nu}:\ \Gamma_{Z2}(Z\to\nu_R\nu_R) = \frac{1}{12\pi}\left(\frac{m_z v}{\Lambda^3}\right)^2(m_z^2+2m_\nu^2)\sqrt{m_z^2-4m_\nu^2}. \quad (27)$$

(We made an $O(1)$ change in the operator coefficients in order to have a uniform normalization of the three-legged vertices.)

The invisible Z-decay width in the standard model is $\Gamma(Z\to{\rm inv}) = 499 \pm 1.5$ MeV [29]. If the Z decay to right-handed neutrinos is kinematically allowed, then, at 3σ, $\Gamma_{Z1,Z2} < 4.5$ MeV gives the contours plotted in Fig. 10. We see from this that the strictest limits on Λ are obtained when the right-handed neutrino mass is small:

[7]Type I involves fermion isosinglets, and the corresponding effective operators would not have tree-level couplings to the W.

TABLE VII. Dimension-7 operators containing right-handed neutrinos, their unitary-gauge expressions, and the vertices with three fields that they contain. We defined $F_{\mu\nu} = \partial_\mu A_\nu - \partial_\nu A_\mu$, $W^+_{\mu\nu} = \partial_\mu W^+_\nu - \partial_\nu W^+_\mu$, and $Z_{\mu\nu} = \partial_\mu Z_\nu - \partial_\nu Z_\mu$. g and g' denote, respectively, the $SU(2)_L$ and $U(1)_Y$ gauge coupling constants.

$\mathcal{O}$ (see Sec. II)	Unitary gauge expression	Three-legged vertices in $\mathcal{O}$ (unitary gauge)
$\frac{1}{2}(\overline{\nu^c}\gamma^\mu E)(\phi\epsilon\overleftrightarrow{D}_\mu\phi)$	$-\frac{i}{2}g(v+H)^3\overline{\nu^c}\not{W}^+P_L e$	$-im_w v^2\overline{\nu^c}\not{W}^+P_L e$
$\frac{1}{2}(\overline{\nu^c}\gamma^\mu N)(i\phi^\dagger\overleftrightarrow{D}_\mu\phi)$	$\frac{1}{\sqrt{8}}(H+v)^3\overline{\nu^c}\not{Z}P_L\nu$	$\frac{v^3}{2\sqrt{2}}\overline{\nu^c}\not{Z}P_L\nu$
$(\overline{\nu^c}\gamma^\mu N)(\partial_\mu\lvert\phi\rvert^2)$	$-\frac{1}{\sqrt{2}}(H+v)^2\partial_\mu H(\overline{\nu^c}\gamma^\mu P_L\nu)$	$-\frac{v^2}{\sqrt{2}}\partial_\mu H(\overline{\nu^c}\gamma^\mu P_L\nu)$
$(\overline{\nu^c}\sigma^{\mu\nu}e)(\phi\epsilon\tau^I\phi)W^I_{\mu\nu}$	$\sqrt{2}(H+v)^2[\partial_\mu W^+_\nu - i(eA_\mu + gc_w Z_\mu)W^+_\nu](\overline{\nu^c}\sigma^{\mu\nu}P_R e)$	$\frac{v^2}{\sqrt{2}}W^+_{\mu\nu}(\overline{\nu^c}\sigma^{\mu\nu}P_R e)$
$\lvert\phi\rvert^2(\overline{\nu^c}\sigma^{\mu\nu}\nu)B_{\mu\nu}$	$\frac{1}{2}(H+v)^2(\overline{\nu^c}\sigma^{\mu\nu}P_R\nu)(c_w F_{\mu\nu} - s_w Z_{\mu\nu})$	$\frac{1}{2}v^2(\overline{\nu^c}\sigma^{\mu\nu}P_R\nu)(c_w F_{\mu\nu} - s_w Z_{\mu\nu})$
$(\overline{\nu^c}D_\mu e)(\phi\epsilon D^\mu\phi)$	$\frac{g}{\sqrt{2}}(v+H)^2[-i(\overline{\nu^c}\partial^\mu P_R e)W^+_\mu + (\overline{\nu^c}P_R e)W^+\cdot(eA - g's_w Z)]$	$-i\sqrt{2}m_w v W^+_\mu(\overline{\nu^c}\partial^\mu P_R e)$
$(\overline{\nu^c}\nu)\lvert D\phi\rvert^2$	$\frac{1}{2}(\overline{\nu^c}P_R\nu)\{[\partial H + i\frac{m_z}{v}(H+v)Z]^2 + \frac{1}{2}g^2(v+H)^2 m_w^2 W^+\cdot W^-\}$	$\cdots$
$(\overline{\nu^c}\nu)\lvert\phi\rvert^4$	$\frac{1}{4}(H+v)^4(\overline{\nu^c}P_R\nu)$	$v^3 H(\overline{\nu^c}P_R\nu)$

$$Z1(m_\nu \ll m_z):\ \Lambda > 354\ \text{GeV},$$
$$Z2(m_\nu \ll m_z):\ \Lambda > 358\ \text{GeV}. \quad (28)$$

B. Operators with right-handed neutrinos contributing to H-invisible decay

Again referring to Table VII, we see that there is a single operator of this type:

$$\overline{\nu^c}\nu|\phi|^4 \supset v^3 H(\overline{\nu^c}P_R\nu), \quad (29)$$

which yields the following invisible decay width:

$$\Gamma(H\to\nu_R\nu_R) = \frac{1}{16\pi}m_H(v/\Lambda)^6\left(1-\frac{2m_\nu^2}{m_H^2}\right)\sqrt{1-\frac{4m_\nu^2}{m_H^2}}. \quad (30)$$

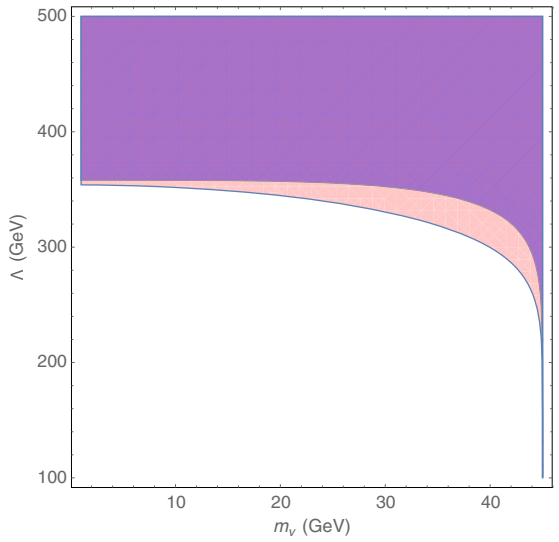

FIG. 10. Z-invisible decay limit on neutrino mass m_ν versus the new physics scale Λ plane derived from Eq. (28). The light red region and above is allowed by the operator $\overline{\nu^c}\not{Z}P_L\nu$, and the lilac region is allowed by $(\overline{\nu^c}\sigma^{\mu\nu}P_{L,R}\nu)Z_{\mu\nu}$.

Using the limit $\mathrm{Br}(H\to\mathrm{inv}) < 0.3$ [50], and $\Gamma_H^{\mathrm{SM}} = 4$ MeV for the total SM contribution to the H width, we find $\Gamma(H\to\mathrm{inv}) < 1.7$ MeV, which we plot in Fig. 11. For light neutrinos, this implies

$$\Lambda > 828\ \text{GeV}, \qquad (m_\nu \ll m_H). \quad (31)$$

C. Operators with right-handed neutrinos contributing to W-leptonic decay

There are three such operators (see Table VII):

$$\frac{1}{2}(\overline{\nu^c}\gamma^\mu E)(\phi\epsilon\overleftrightarrow{D}_\mu\phi) \supset -im_w v^2\overline{\nu^c}\not{W}^+P_L e,$$
$$(\overline{\nu^c}\sigma^{\mu\nu}e)(\phi\epsilon\tau^I\phi)W^I_{\mu\nu} \supset \sqrt{2}v^2(\partial_\mu W^+_\nu)(\overline{\nu^c}\sigma^{\mu\nu}P_R e),$$
$$(\overline{\nu^c}D_\mu e)(\phi\epsilon D^\mu\phi) \supset -i\sqrt{2}m_w v W^+_\mu(\overline{\nu^c}\partial^\mu P_R e), \quad (32)$$

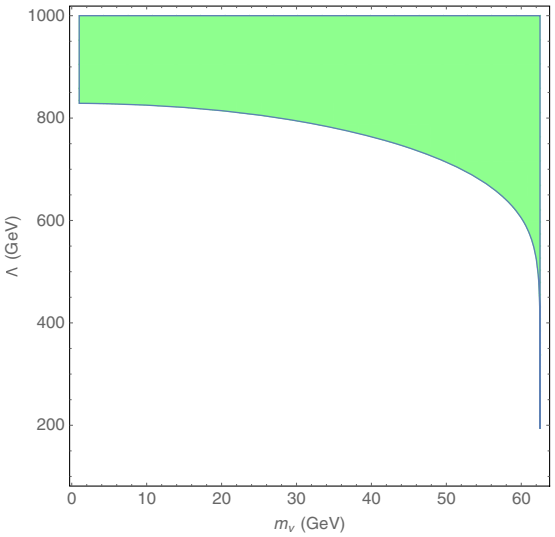

FIG. 11. H-invisible decay limit on neutrino mass m_ν versus the new physics scale Λ plane derived from Eq. (30). The shaded region is allowed by the operator $\overline{\nu^c}\nu|\phi|^4$.

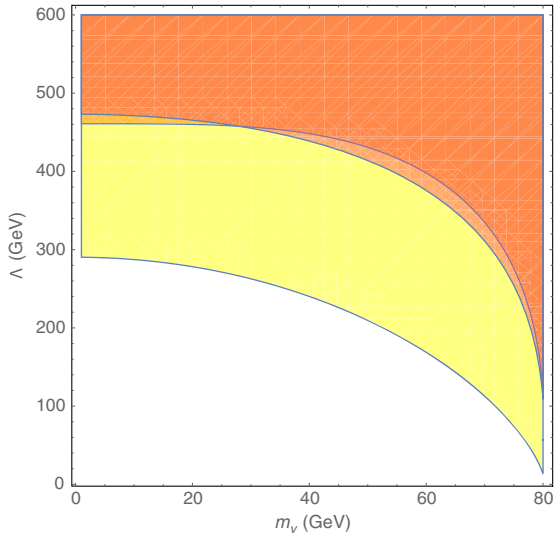

FIG. 12. W-decay limit on neutrino mass m_ν versus the new physics scale Λ plane derived from Eq. (33). The yellow region and above is allowed by $W^+_\mu(\overline{\nu^c}\partial^\mu P_R e)$, the darker orange region and above is allowed by $(\overline{\nu^c}\sigma^{\mu\nu}P_R e)\partial_\mu W^+_\nu$, and the orange region and above is allowed by $\overline{\nu^c}W^+P_L e$.

that lead to three contributions to the leptonic W-decay width:

$$\begin{aligned}
&\frac{m_{\rm w}v^2}{\Lambda^3}\overline{\nu^c}W^+P_L e\colon \Gamma_{W1}\\
&\quad=\frac{1}{192\pi}\left(\frac{v^4}{\Lambda^6 m_{\rm w}^3}\right)(m_{\rm w}^2-m_\nu^2)^2(2m_{\rm w}^2+m_\nu^2),\\
&\frac{m_{\rm w}v}{\Lambda^3}(\partial_\mu W^+_\nu)(\overline{\nu^c}\sigma^{\mu\nu}P_R e)\colon \Gamma_{W2}\\
&\quad=\frac{1}{12\pi}\left(\frac{v^2}{\Lambda^6 m_{\rm w}}\right)(m_{\rm w}^2-m_\nu^2)^2(m_{\rm w}^2+2m_\nu^2),\\
&\frac{m_{\rm w}v}{\Lambda^3}W^+_\mu(\overline{\nu^c}\partial^\mu P_R e)\colon \Gamma_{W3}=\frac{1}{192\pi}\left(\frac{v^2}{\Lambda^6 m_{\rm w}^3}\right)(m_{\rm w}^2-m_\nu^2)^4.
\end{aligned} \tag{33}$$

Now, the branching fraction of W to $\ell+\nu_\ell$ (combined leptonic final states) is $\Gamma(W\to\ell\nu_\ell)/\Gamma_W=(10.86\pm 0.09)\%$ with $\Gamma_W=2.085$ GeV [29]. This produces the contours of Fig. 12 in the 3σ limit; for light neutrinos,

$$\begin{aligned}
&W1(m_\nu\ll m_{\rm w})\colon \Lambda>473\ \text{GeV},\\
&W2(m_\nu\ll m_{\rm w})\colon \Lambda>460\ \text{GeV},\\
&W3(m_\nu\ll m_{\rm w})\colon \Lambda>290\ \text{GeV}.
\end{aligned} \tag{34}$$

D. Operators contributing to the neutrino magnetic moment

The operators relevant for this constraint are listed in Eq. (B1), for which the most significant constraint is derived from the cooling rate of red giants and other astrophysical objects [30]. Using the results in Ref. [20], we find that the strongest restriction is obtained by requiring that the process $\gamma+\nu_{\rm light}\to\nu_{\rm heavy}$ not be a very efficient cooling mechanism in supernovae [30]:

$$\Lambda>\left(1-\frac{4m_\nu^2}{\omega_P^2}\right)^{1/4}\times 47\ \text{TeV},\qquad 2m_\nu\le\omega_P\simeq 30\ \text{MeV}, \tag{35}$$

where ω_P is the typical supernova plasma frequency; this same limit is often expressed by the constraint that the ν magnetic moment is smaller than $3\times10^{-12}\mu_B$. The shaded region in Fig. 13 shows the allowed range of NP scale (Λ) as a function of neutrino mass (m_ν) from neutrino magnetic moment constraint as in Eq. (35).

There are no important limits on Λ for magnetic coupling for larger neutrino masses; in particular, collider data are useful only when the underlying physics is assumed to be strongly coupled. For weakly coupled heavy physics, the effective operator coefficients are too small to produce a measurable effect given the experimental sensitivity [20].

When the above decays are forbidden, or when the operator does not have three-legged vertices, the experimental constraints are degraded. This is because in this case existing limits are obtained within the context of specific models and cannot be directly extended to limits on all effective operator coefficients. For example, there are strict limits on the masses of the right-handed neutrinos and the right-handed W_R gauge bosons present in L-R models [51]. But these do not translate to limits on m_ν or Λ (when the W_R and extra scalars are assumed to be heavy, with masses $\sim\Lambda$), since the leading effective operators (obtained after integration of these heavy particles), whose effects are strongly constrained by experiment, are *not* the ones being considered here. The simplest way of seeing this is to note that all our operators violate lepton number, so within such L-R models they will appear multiplied by small coefficients (e.g., by the small vacuum expectation value of a scalar triplet [52]) and will have subdominant effects. The point is that without knowledge of the model realized in nature, one cannot, in general, use limits obtained using some operators to constrain the effects of others. A full analysis of the potential collider reactions that can best probe the operators in Table VII lies beyond the scope of this paper.

VI. CONCLUSIONS

In this paper, we have worked out all possible effective operators of dimension 7 involving SM fields and right-handed neutrinos, indicating those that could be generated at tree level by the underlying theory, and which may then contribute significantly to low-energy observables. Our results generalize lists of dimension-7 operators involving

only SM fields [15], as well as earlier partial compilations [17]. All dimension-7 operators violate $B-L$ by 2 units.

From the operators presented, we selected two that can generate clear dilepton and trilpeton signatures at the LHC. The current limit on the scale of new physics is $\simeq$330 GeV [Eq. (22)], while the sensitivity to the scale of new physics can reach $\simeq$460 GeV [Eq. (24)], with the dilepton channel providing the highest sensitivity. We argue that these results correspond to sensitivity to the presence of heavy fermion triplets (which can also be responsible for the type-III seesaw mechanism for generating neutrino masses) and are competitive with the ones obtained from direct production. We argued that these limits are not necessarily superseded by the stronger ones derived from precision data given the inability to account for cancellations in the latter.

We have also obtained limits on the NP scale of operators containing right-handed neutrinos from Z, H, W decays, which are of the order of $\sim$500 GeV or less for Z, W semileptonic decays; limits on the H-invisible decay give a stronger limit $\sim$800 GeV (all with a dependence on the right-handed neutrino mass). As for the light neutrinos, much stronger constraints are obtained from the magnetic-moment effective operator, but only for small ($<$30 MeV) masses.

Finally, we note that effective Lagrangian models have recently gained interest when studying the LHC sensitivity to various dark matter models; see, for example, Ref. [53].

ACKNOWLEDGMENTS

The work of S. B. is partially funded by DST-INSPIRE Grant No. PHY/P/SUB/01 at IIT Guwahati.

APPENDIX A: LOOP-GENERATED AND POTENTIALLY TREE-GENERATED OPERATORS

In this appendix, we present the arguments for determining whether an operator is necessarily generated by heavy physics loops (LG operators), or if there are types of new physics that can generate the operator at tree level (potentially tree-generated or PTG operators). As throughout this paper, we assume the NP is weakly coupled, and decoupling, and that the full theory is renormalizable. In this case, denoting by I, E the number of internal and external lines, respectively; by L the number of loops; and by V_n the number of vertices with n legs, we have the well-known relations

$$L = I - V + 1, \qquad \sum_{n\geq 3} nV_n = 2I + E, \qquad V = \sum_{n\geq 3} V_n, \tag{A1}$$

which for tree graphs ($L=0$) in renormalizable theories ($V_{n\geq 5}=0$) imply

$$V_3 + 2V_4 = E - 2. \tag{A2}$$

When needed, we will denote a heavy fermion by Ψ, a heavy scalar by Φ, and a heavy vector by V; correspondingly, we denote SM vectors, fermions and scalars by A, ψ and φ, respectively.

We will also need some basic properties of the couplings of matter and vector fields in gauge theories. We denote by the index l a gauge direction associated with a light (SM) vector boson, while an index h will be associated with the heavy gauge-boson directions. Accordingly, the generators are denoted T^l and T^h, and the group structure constants take the generic form $f_{lll,llh,lhh,hhh}$. The group generators in general connect light and heavy particle (fermion and scalar) directions; these we also denote by the subindices l and h: $(T^h)_{ll}$, $(T^h)_{lh}$, $(T^h)_{hl}$, $(T^h)_{hh}$, and similarly for T^l. General properties of gauge theories imply that

$$f_{llh} = 0, \qquad (T^l)_{lh} = (T^l)_{hl} = 0. \tag{A3}$$

Since a vacuum expectation value $\langle\Phi\rangle$ does not break the electroweak symmetry, we also have

$$T^l\langle\Phi\rangle = 0. \tag{A4}$$

Also, since $T^h\langle\Phi\rangle$ is a vector in the direction of a would-be Goldstone boson, it follows that

$$(T^h\langle\Phi\rangle)_l = 0. \tag{A5}$$

We now use these relations to determine the LG or PTG character of the operators listed in Sec. II:

(1) ψ^2D^4 *operators*. These are of the form $\nu^2 A_{\mu\nu}A_{\rho\sigma}$ or $\nu^2 A_{\mu\nu}\tilde{A}_{\rho\sigma}$, and it is straightforward to see that the possible tree diagrams involve a heavy vector, scalar or fermion.
   (a) Heavy fermion exchange: The graphs have a $\nu\Psi A$ vertex and are then proportional to $(T^l)_{lh}=0$, because of Eq. (A3).
   (b) Heavy vector exchange: The graphs have an AAV vertex and are then proportional to $f_{llh}=0$, because of Eq. (A3).
   (c) Heavy scalar exchange: The graphs have an $AA\Phi$ vertex, and are then proportional to $\langle\Phi\rangle\{T^l,T^{l'}\}\Phi'=0$, because of Eq. (A4).

(2) $\psi^2D^3\varphi$ *operators*. These are of the form $\partial^\mu\psi\gamma^\nu\varphi\psi A_{\mu\nu}$ or $\partial^\mu\psi\gamma^\nu\varphi\psi\tilde{A}_{\mu\nu}$, and the possible tree diagrams involve a heavy vector, scalar or fermion.
   (a) Heavy fermion exchange: The graphs have a $\psi\Psi A$ vertex, and are then proportional to $(T^l)_{lh}=0$, because of Eq. (A3).
   (b) Heavy vector exchange: The graphs have a φAV vertex, and are then proportional to $\langle\Phi\rangle\{T^l,T^h\}\varphi=0$, because of Eqs. (A4) and (A5).

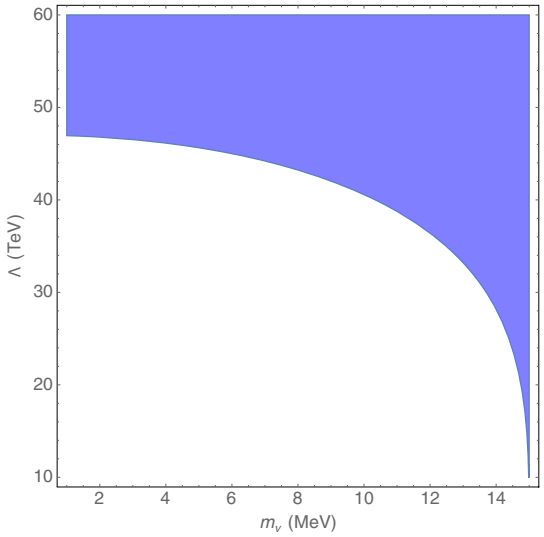

FIG. 13. Shaded area: Region in the neutrino mass m_ν (GeV) versus the new physics scale Λ (GeV) plane allowed by the neutrino magnetic moment constraint [Eq. (35)].

(c) Heavy scalar exchange: The graphs have an $A\varphi\Phi$ vertex, which is proportional to $(T^l)_{hl} = 0$, because of Eq. (A3).

(3) $\psi^2 D^2\varphi^2$ *operators*. These separate into two categories according to whether D^2 represents a field tensor $D^2 \to A_{\mu\nu}$ or not. Both cases can be generated at tree level by the heavy-fermion exchange diagrams ❶ and ❷ in Fig. 14. None of the vertices in these graphs are *a priori* forbidden by the gauge symmetry (though they give rise to mixing among light and heavy fermions and the associated naturality issues).

There are three operators in this group, $\mathcal{O}_{1,3,4}$, that are associated with the type I, II and III seesaw neutrino mass generation mechanism. To see this relation explicitly, we define

$$\mathcal{O}'_I = (\ell\phi)\Box(\ell\phi), \qquad \mathcal{O}'_{II} = (\ell\boldsymbol{\tau}\ell)D^2(\phi\boldsymbol{\tau}\phi),$$
$$\mathcal{O}'_{III} = (\ell\boldsymbol{\tau}\phi)D^2(\ell\boldsymbol{\tau}\phi), \tag{A6}$$

which can be generated by the exchange of a fermion isosinglet, a scalar isotriplet or a fermion isotriplet, respectively; the relevant graphs are given in Fig. 14. Using the equations of motion (as allowed by the equivalence theorem, see Sec. I), we find that these two sets of operators are equivalent:

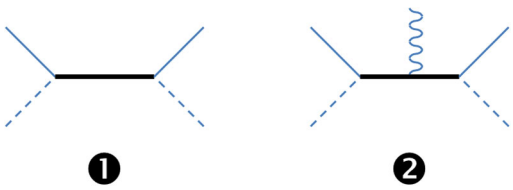

FIG. 14. Diagrams that generate operators of the form $\psi^2 D^2\varphi^2$ at tree level [thick lines denote particles with (Λ) masses].

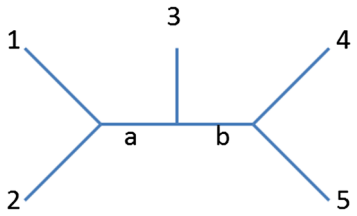

FIG. 15. Tree-level graph that can generate operators of the form $\psi^4 D$; the lines labeled "a" and "b" correspond to heavy particles (see text for details).

$$\begin{pmatrix} \mathcal{O}'_I \\ \mathcal{O}'_{II} \\ \mathcal{O}'_{III} \end{pmatrix} = \begin{pmatrix} 0 & 0 & 2 \\ 8 & 4 & 8 \\ -2 & 0 & -6 \end{pmatrix} \begin{pmatrix} \mathcal{O}_1 \\ \mathcal{O}_3 \\ \mathcal{O}_4 \end{pmatrix}. \tag{A7}$$

The advantage of the primed basis is that it manifestly depicts the type of particles that generate them and nicely matches them to the usual seesaw graphs associated with neutrino mass generation.

Now, because $\mathcal{O}_{1,3}$ contain the term $m_w^2 W^{+2} e_L^2$ ($\mathcal{O}_2$ does not), $\mathcal{O}'_{II,III}$ will also have such interactions. The validity of the EFT for $\mathcal{O}'_{II}$ requires that the dilepton invariant mass satisfy $M_{\ell\ell} \ll \Lambda$, while for $\mathcal{O}'_{III}$ the W lepton should be similarly bound: $M_{\ell W} \ll \Lambda$.

(4) $\psi^2 D\varphi^3$ *operators*. These contain vertices with two fermions and three scalars, and it is easy to see that they can be generated at tree level, for example by Ψ exchange.

(5) $\psi^2\varphi^4$ *operators*. These contain vertices with two fermions and four scalars,. The tree-level graphs then satisfy[8] $V_3 + 2V_4 = 4$, so that $V_3 = 2$, $V_4 = 1$ or $V_3 = 4$, and the first class of graphs can generate the operators at tree level (vertices: $\psi^2\Phi$, $\Phi^2\varphi$, $\varphi^3\Phi$, and two internal Φ lines).

(6) $\psi^4 D$ *operators*. These contain a vertex $\psi^4 A$, which corresponds to tree-level graphs with $E = 5$ and $V_3 = 3$, $V_4 = 0$, or $V_3 = V_4 = 1$, but the latter do not occur since the underlying (renormlizable) theory does not contain four-legged vertices with fermions; the graphs are those in Fig. 15, where

Case	1	2	3	4	5	a	b
i	ψ	ψ	A	ψ	ψ	Φ	Φ
ii	ψ	ψ	A	ψ	ψ	V	V
iii	ψ	ψ	A	ψ	ψ	V	Φ
iv	X	ψ	ψ	ψ	ψ	Ψ	V
v	X	ψ	ψ	ψ	ψ	Ψ	Φ

(A8)

(a) Case i contains the vertex $\Phi\Phi X$, which has a derivative, so the operators generated by

[8]The case $V_4 = 2$ does not occur, because in renormalizable theories there are no four-legged vertices with fermions.

such graphs are of the form $\psi^4 X\partial$ and are of dimension 8.

(b) Case *ii* contains the vertex VVA with one derivative and also corresponds to operators of dimension 8.

(c) Case *iii* contains the vertex $XV\Phi$ of the form which vanishes because of Eqs. (A4) and (A5).

(d) Cases *iv* and *v* require the vertex $\psi X\Psi$, which does not exist because of Eq. (A3).

If follows that all these are LG operators.

$\psi^4\varphi$ operators: Since fourr-fermion interactions can be tree-generated by exchange of a heavy boson, operators of the form $\psi^4\varphi$ can be obtained by attaching a φ to the internal heavy boson line. These are all PTG operators.

APPENDIX B: PTG OPERATORS CONTAINING RIGHT-HANDED NEUTRINOS

The dimension-7 PTG operators containing right-handed neutrinos (see Sec. II) are listed in Table VII.

It follows from this list that there are eight types of three-legged vertices involving right-handed neutrinos and contributing to the Z, H, W decays and neutrino magnetic moments:

	SM-like coupling	Derivative coupling	Magnetic coupling
Z	$\overline{\nu^c} \not{Z} P_L \nu$	$\cdots$	$(\overline{\nu^c}\sigma^{\mu\nu}P_R\nu)Z_{\mu\nu}$
H	$H(\overline{\nu^c}P_R\nu)$	$\partial_\mu H(\overline{\nu^c}\gamma^\mu P_L\nu)$	$\cdots$
W	$\overline{\nu^c}\not{W}^+ P_L e$	$W^+_\mu(\overline{\nu^c}\partial^\mu P_R e)$	$(\overline{\nu^c}\sigma^{\mu\nu}P_R e)W^+_{\mu\nu}$
γ	$\cdots$	$\cdots$	$(\overline{\nu^c}\sigma^{\mu\nu}P_R\nu)F_{\mu\nu}$

(B1)

The most significant constraints on Λ derived from these vertices were derived in Sec. V.

[1] See, for example, M. C. Gonzalez-Garcia and Y. Nir, Neutrino masses and mixing: Evidence and implications, Rev. Mod. Phys. **75**, 345 (2003); R. Mohapatra, S. Antusch, K. Babu, G. Barenboim, M.-C. Chen *et al.*, Theory of neutrinos: A white paper, Rep. Prog. Phys. **70**, 1757 (2007).

[2] See, for example, G. Bertone, D. Hooper, and J. Silk, Particle dark matter: Evidence, candidates and constraints, Phys. Rep. **405**, 279 (2005).

[3] See, for example, J. Polchinski, Effective field theory and the Fermi surface, in Boulder 1992, Proceedings, Recent Directions in Particle Theory, pp. 235–274, and Calif. Univ. Santa Barbara Report No. NSF-ITP-92-132 (1992), and Texas Univ. Austin Report No. UTTG-92-20 (1992).

[4] K. G. Wilson and J. B. Kogut, The renormalization group and the epsilon expansion, Phys. Rep. **12**, 75 (1974).

[5] S. Weinberg, Phenomenological Lagrangians, Physica A (Amsterdam) **96**, 327 (1979); for a pedagogical review, see A. Dobado, A. Gomez-Nicola, A. L. Maroto, and J. R. Pelaez, *Effective Lagrangians for the Standard Model* (Springer, New York, 1997).

[6] H. Georgi, On-shell effective field theory, Nucl. Phys. **B361** (1991) 339; J. Wudka, Electroweak effective Lagrangians, Int. J. Mod. Phys. A **09**, 2301 (1994); C. Arzt, Reduced effective Lagrangians, Phys. Lett. B **342**, 189 (1995).

[7] G. 't Hooft and M. J. G. Veltman, Regularization and renormalization of gauge fields, Nucl. Phys. **B44**, 189 (1972).

[8] T. Appelquist and J. Carazzone, Infrared singularities and massive fields, Phys. Rev. D **11**, 2856 (1975); for a pedagogical introduction, see J. Collins, *Renormalization: An Introduction to Renormalization, the Renormalization Group and the Operator-Product Expansion* (Cambridge University Press, Cambridge, England, 1986).

[9] G. C. Branco, P. M. Ferreira, L. Lavoura, M. N. Rebelo, M. Sher, and J. P. Silva, Theory and phenomenology of two-Higgs-doublet models, Phys. Rep. **516**, 1 (2012).

[10] K. Agashe, R. Contino, and A. Pomarol, The minimal composite Higgs model, Nucl. Phys. **B719**, 165 (2005).

[11] M. J. G. Veltman, The infrared-ultraviolet connection, Acta Phys. Pol. B **12**, 437 (1981).

[12] S. Weinberg, Baryon and Lepton Nonconserving Processes, Phys. Rev. Lett. **43**, 1566 (1979).

[13] W. Buchmuller and D. Wyler, Effective Lagrangian analysis of new interactions and flavor conservation, Nucl. Phys. **B268**, 621 (1986).

[14] B. Grzadkowski, M. Iskrzynski, M. Misiak, and J. Rosiek, Dimension-Six terms in the standard model Lagrangian, J. High Energy Phys. 10 (2010) 085.

[15] L. Lehman, Extending the standard model effective field theory with the complete set of dimension-7 operators, Phys. Rev. D **90**, 125023 (2014).

[16] K. S. Babu and C. N. Leung, Classification of effective neutrino mass operators, Nucl. Phys. **B619**, 667 (2001); A. de Gouvea and J. Jenkins, A survey of lepton number

violation via effective operators, Phys. Rev. D **77**, 013008 (2008); F. Bonnet, D. Hernandez, T. Ota, and W. Winter, Neutrino masses from higher than $d = 5$ effective operators, J. High Energy Phys. 10 (2009) 076; P. W. Angel, N. L. Rodd, and R. R. Volkas, Origin of neutrino masses at the LHC: $\Delta L = 2$ effective operators and their ultraviolet completions, Phys. Rev. D **87**, 073007 (2013); C. Degrande, A basis of dimension-eight operators for anomalous neutral triple gauge boson interactions, J. High Energy Phys. 02 (2014) 101.

[17] S. Weinberg, Varieties of baryon and lepton nonconservation, Phys. Rev. D **22**, 1694 (1980); K. S. Babu and R. N. Mohapatra, $B - L$ Violating Proton Decay Modes and New Baryogenesis Scenario in $SO(10)$, Phys. Rev. Lett. **109**, 091803 (2012); K. S. Babu and R. N. Mohapatra, $B - L$ violating nucleon decay and GUT scale baryogenesis in $SO(10)$, Phys. Rev. D **86**, 035018 (2012); G. Chalons and F. Domingo, Dimension 7 operators in the b to s transition, Phys. Rev. D **89**, 034004 (2014).

[18] H. A. Weldon and A. Zee, Operator analysis of new physics, Nucl. Phys. **B173**, 269 (1980); C. Arzt, M. B. Einhorn, and J. Wudka, Effective Lagrangian approach to precision measurements: The anomalous magnetic moment of the muon, Phys. Rev. D **49**, 1370 (1994); S. Bar-Shalom, A. Soni, and J. Wudka, EFT naturalness: An effective field theory analysis of Higgs naturalness, arXiv:1405.2924; S. Dawson, I. M. Lewis, and M. Zeng, Effective field theory for Higgs boson plus jet production, Phys. Rev. D **90**, 093007 (2014); R. Catena, Prospects for direct detection of dark matter in an effective theory approach, J. Cosmol. Astropart. Phys. 07 (2014) 055; S. Matsumoto, S. Mukhopadhyay, and Y. L. S. Tsai, Singlet Majorana fermion dark matter: A comprehensive analysis in effective field theory, J. High Energy Phys. 10 (2014) 155; G. M. Pruna and A. Signer, The $\mu \to e\gamma$ decay in a systematic effective field theory approach with dimension 6 operators, J. High Energy Phys. 10 (2014) 14; A. Biektter, A. Knochel, M. Krmer, D. Liu, and F. Riva, Vices and virtues of Higgs effective field theories at large energy, Phys. Rev. D **91**, 055029 (2015); M. Duch, B. Grzadkowski, and J. Wudka, Classification of effective operators for interactions between the standard model and dark matter, J. High Energy Phys. 05 (2015) 116.

[19] See, for example, A. Zee, A theory of lepton number violation, neutrino Majorana mass, and oscillation, Phys. Lett. **93B**, 389 (1980); **95B**, 461(E) (1980).

[20] A. Aparici, K. Kim, A. Santamaria, and J. Wudka, Right-handed neutrino magnetic moments, Phys. Rev. D **80**, 013010 (2009).

[21] F. del Aguila, S. Bar-Shalom, A. Soni, and J. Wudka, Heavy majorana neutrinos in the effective Lagrangian description: Application to hadron colliders, Phys. Lett. B **670**, 399 (2009).

[22] See, for example, J. D. Vergados, The neutrinoless double beta decay from a modern perspective, Phys. Rep. **361**, 1 (2002); F. del Aguila, A. Aparici, S. Bhattacharya, A. Santamaria, and J. Wudka, Effective Lagrangian approach to neutrinoless double beta decay and neutrino masses, J. High Energy Phys. 06 (2012) 146.

[23] C. Arzt, M. B. Einhorn, and J. Wudka, Patterns of deviation from the standard model, Nucl. Phys. **B433**, 41 (1995).

[24] See, for example, M. Spira, A. Djouadi, D. Graudenz, and P. M. Zerwas, Higgs boson production at the LHC, Nucl. Phys. **B453**, 17 (1995); M. B. Einhorn and J. Wudka, Higgs-boson couplings beyond the Standard Model, Nucl. Phys. **B877**, 792 (2013).

[25] M. B. Einhorn and J. Wudka, The bases of effective field theories, Nucl. Phys. **B876**, 556 (2013).

[26] A. de Gouvea, J. Herrero-Garcia, and A. Kobach, Neutrino masses, grand unification, and baryon number violation, Phys. Rev. D **90**, 016011 (2014).

[27] J. D. Vergados, H. Ejiri, and F. Simkovic, Theory of neutrinoless double beta decay, Rep. Prog. Phys. **75**, 106301 (2012).

[28] See F. del Aguila, A. Aparici, S. Bhattacharya, A. Santamaria, and J. Wudka, Effective Lagrangian approach to neutrinoless double beta decay and neutrino masses, J. High Energy Phys. 06 (2012) 146, and references therein.

[29] K. A. Olive *et al.* (Particle Data Group Collaboration), Review of particle physics, Chin. Phys. C **38**, 090001 (2014).

[30] V. Castellani and S. Degl'Innocenti, Stellar evolution as a probe of neutrino properties, Astrophys. J. **402**, 574 (1993); M. Catelan, J. A. d. F. Pacheco, and J. E. Horvath, The helium-core mass at the helium flash in low-mass red giant stars: Observations and theory, Astrophys. J. **461**, 231 (1996); M. Haft, G. Raffelt, and A. Weiss, Standard and nonstandard plasma neutrino emission revisited, Astrophys. J. **425**, 222 (1994); **438**, 1017(E) (1995); G. G. Raffelt, Core mass at the helium flash from observations and a new bound on neutrino electromagnetic properties, Astrophys. J. **365**, 559 (1990); New Bound on Neutrino Dipole Moments from Globular Cluster Stars, Phys. Rev. Lett. **64**, 2856 (1990); G. Raffelt and A. Weiss, Nonstandard neutrino interactions and the evolution of red giants, Astron. Astrophys. **264**, 536 (1992); A. Heger, A. Friedland, M. Giannotti, and V. Cirigliano, The impact of neutrino magnetic moments on the evolution of massive stars, Astrophys. J. **696**, 608 (2009); The impact of neutrino magnetic moments on the evolution of massive stars, *Astrophys. J.* 696, 608 (2009). G. G. Raffelt, *Stars as Laboratories for Fundamental Physics: The Astrophysics of Neutrinos, Axions, and Other Weakly Interacting Particles* (University of Chicago, Chicago, 1996), p. 664; N. Iwamoto, L. Qin, M. Fukugita, and S. Tsuruta, Neutrino magnetic moment and neutron star cooling, Phys. Rev. D **51**, 348 (1995); G. G. Raffelt, Limits on neutrino electromagnetic properties: An update, Phys. Rep. **320**, 319 (1999).

[31] F. del Aguila, A. Aparici, S. Bhattacharya, A. Santamaria, and J. Wudka, A realistic model of neutrino masses with a large neutrinoless double beta decay rate, J. High Energy Phys. 05 (2012) 133.

[32] A. Belyaev, N. D. Christensen, and A. Pukhov, CalcHEP 3.4 for collider physics within and beyond the standard model, Comput. Phys. Commun. **184**, 1729 (2013).

[33] H. L. Lai, J. Huston, S. Kuhlmann, J. Morfin, F. Olness, J. F. Owens, J. Pumplin, and W. K. Tung (CTEQ Collaboration),

Global QCD analysis of parton structure of the nucleon: CTEQ5 parton distributions, Eur. Phys. J. C **12**, 375 (2000).
[34] ATLAS Collaboration, Physics at a high-luminosity LHC with ATLAS, arXiv:1307.7292.
[35] J. Varela (CMS Collaboration), Prospects for physics at high luminosity with CMS, EPJ Web Conf. **49**, 11003 (2013).
[36] ATLAS Collaboration, Physics at a high-luminosity LHC with ATLAS, Report No. ATL-PHYS-PUB-2012-001.
[37] ATLAS, CDF, CMS, and D0 collaborations, First combination of Tevatron and LHC measurements of the top-quark mass, arXiv:1403.4427.
[38] T. Sjostrand, S. Mrenna, and P. Skands, PYTHIA 6.4 physics and manual, J. High Energy Phys. 05 (2006) 026.
[39] V. Khachatryan *et al.* (CMS Collaboration), First measurement of the cross section for top-quark pair production in proton-proton collisions at $\sqrt{s} = 7$ TeV, Phys. Lett. B **695**, 424 (2011).
[40] A. Calderon (ATLAS and CMS collaborations), Top pair cross section measurements at the LHC, arXiv:1301.1158.
[41] S. Moch and P. Uwer, Theoretical status and prospects for top-quark pair production at hadron colliders, Phys. Rev. D **78**, 034003 (2008).
[42] S. Chatrchyan *et al.* (CMS Collaboration), Search for new physics in events with same-sign dileptons and jets in pp collisions at $\sqrt{s} = 8$ TeV, J. High Energy Phys. 01 (2014) 163.
[43] R. Foot, H. Lew, X. G. He, and G. C. Joshi, Seesaw neutrino masses induced by a triplet of leptons, Z. Phys. C **44**, 441 (1989).
[44] CMS Physics Analysis Summary, CMS Report No. PAS EXO-11-073.
[45] V. Khachatryan *et al.* (CMS Collaboration), Search for heavy Majorana neutrinos in $\mu^{\pm}\mu^{\pm}+$ jets events in proton-proton collisions at $\sqrt{s} = 8$ TeV, Phys. Lett. B **748**, 144 (2015).
[46] F. del Aguila and J. A. Aguilar-Saavedra, Distinguishing seesaw models at LHC with multi-lepton signals, Nucl. Phys. **B813**, 22 (2009).
[47] R. Franceschini, T. Hambye, and A. Strumia, Type-III seesaw at LHC, Phys. Rev. D **78**, 033002 (2008).
[48] B. Bajc and G. Senjanovic, Seesaw at LHC, J. High Energy Phys. 08 (2007) 014.
[49] See, for example, F. del Aguila, S. Bar-Shalom, A. Soni, and J. Wudka, Heavy Majorana neutrinos in the effective Lagrangian description: Application to hadron colliders, Phys. Lett. B **670**, 399 (2009).
[50] G. Aad *et al.* (ATLAS Collaboration), Search for invisible decays of a Higgs boson using vector-boson fusion in pp collisions at $\sqrt{s} = 8$ TeV with the ATLAS detector, J. High Energy Phys. 01 (2016) 172.
[51] V. Khachatryan *et al.* (CMS Collaboration), Search for heavy neutrinos and W bosons with right-handed couplings in proton-proton collisions at $\sqrt{s} = 8$ TeV, Eur. Phys. J. C **74**, 3149 (2014).
[52] M. Dhuria, C. Hati, R. Rangarajan, and U. Sarkar, Falsifying leptogenesis for a TeV scale $W_R^{\pm}$ at the LHC, Phys. Rev. D **92**, 031701 (2015).
[53] J. Goodman, M. Ibe, A. Rajaraman, W. Shepherd, T. M. P. Tait, and H. B. Yu, Constraints on dark matter from colliders, Phys. Rev. D **82**, 116010 (2010); G. Busoni, A. De Simone, J. Gramling, E. Morgante, and A. Riotto, On the validity of the effective field theory for dark matter searches at the LHC, part II: Complete analysis for the s-channel, J. Cosmol. Astropart. Phys. 06 (2014) 060; On the validity of the effective field theory for dark matter searches at the LHC, part III: Analysis for the t-channel, J. Cosmol. Astropart. Phys. 09 (2014) 022; J. Abdallah, A. Ashkenazi, A. Boveia, G. Busoni, A. De Simone, C. Doglioni, A. Efrati, E. Etzion *et al.*, Simplified models for dark matter and missing energy searches at the LHC, arXiv:1409.2893.